DYNAMIC CHARACTERISTICS OF RUBBER PAD FOR VIBRATION MITIGATION

LAU JIA RONG

A project report submitted in partial fulfilment of the requirements for the award of Bachelor of Engineering (Honours) Mechanical Engineering

Lee Kong Chian Faculty of Engineering and Science
Universiti Tunku Abdul Rahman

September 2022

DECLARATION

I hereby declare that this project report is based on my original work except for citations and quotations which have been duly acknowledged. I also declare that it has not been previously and concurrently submitted for any other degree or award at UTAR or other institutions.

Signature   :

Name   :   Lau Jia Rong

ID No.   :   17UEB04567

Date   :   11st September 2022

APPROVAL FOR SUBMISSION

I certify that this project report entitled **"DYNAMIC CHARACTERISTICS OF RUBBER PAD FOR VIBRATION MITIGATION"** was prepared by **LAU JIA RONG** has met the required standard for submission in partial fulfilment of the requirements for the award of Bachelor of Engineering (Honours) Mechanical Engineering at Universiti Tunku Abdul Rahman.

Approved by,

Signature   :

Supervisor   :   Ts. Dr. King Yeong Jin

Date   :   3 October 2022

ACKNOWLEDGEMENTS

ABSTRACT

Rubber pad is a material that is vastly used in mitigating mechanical vibration. The material composition of a rubber pad is made to determine the dynamic characteristics of the rubber pad. For the best mitigation of vibration to occur, the rubber pad used in certain systems must achieve critical damping. However, critical damping is hard to achieve every time as the dynamic characteristics of the rubber pad is affected by the dynamic load of the system supported by the rubber pad. Although rubber pads are usually produced with a specified range of dynamic properties, end-users often find that the rubber pad does not work within the specified range. The problem arises here is the equipment needed to justify the dynamic properties of the product is unavailable in the market if not relatively expensive. A reliable test rig that is capable of applying preloads on rubber pads has been developed. The test rig utilised the instrumented hammer impact method and the concept of single-degree-of-freedom system in determining the dynamic properties of rubber pads that adapt the dimension of a standard railpad. The dynamic stiffness of rubber pads are found to increase as the applied preload increases. Throughout the range of preload, the store bought EPDM achieved the highest dynamic stiffnesses amongst the three rubber pads, which is from 906 to 951 MN/m, the natural rubber pad followed in second with a range from 625 to 950 MN/m, while the EPDM railpad has the lowest dynamic stiffness with a range from 377 to 840 MN/m. In terms of the damping coefficient, the store bought EPDM has a range from 1305 to 4354 Ns/m, the EPDM railpad has a range from 2340 to 4668 Ns/m, and the natural rubber pad has a range from 1719 to 6868 Ns/m. The grooves profile that the natural rubber pad possesses appeared to aid the rubber pad in stress dissipation when the load applied is slow and steady.

TABLE OF CONTENTS

LIST OF TABLES

LIST OF FIGURES

LIST OF SYMBOLS / ABBREVIATIONS

m_p	effective rail mass, kg
c_p	damping coefficient of rail pad, Ns/m
k_p	dynamic stiffness of rail pad, N/m
ω_n	natural frequency of rail pads, rad/s
ζ	damping ratio
τ	wrench torque, Nm
K	constant that depends on the bolt material and size
F	axial bolt force, N
d	nominal bolt diameter, m
l	lubrication factor, %

EVA	ethylene-vinyl acetate
EPDM	ethylene propylene diene monomer
2DOF	two-degree-of-freedom
SDOF	single-degree-of-freedom
FRF	frequency response function
CAM	cement asphalt mortar
CR	chloroprene rubber
TPE	thermoplastic polyurethane elastomer
EQM	equation of motion

LIST OF APPENDICES

CHAPTER 1

INTRODUCTION

1.1   General Introduction

Vibration is simply the back and forth movement of any single body caused by the translation of kinetic energy between the particles of the body. This movement is known as the oscillation of a vibration. The dynamic of a vibration is usually measured by its frequency and amplitude. Frequency of a vibration is the number of cycle that the vibration completes in one second. Frequency is expressed in the unit of hertz (*Hz*) which is equals to one cycle per second. In simpler words, frequency is known as the speed of a vibration in most cases. Amplitude of a vibration is the maximum displacement of the body move away from its stationary position. If the amplitude of a vibration is measured, it is usually expressed in the unit of metre (*m*) which is the distance from the stationary position to the extreme position on both direction of the vibration. However, in most cases amplitude are used in measuring the loudness of a sound, which understandaly caused by the vibration of a medium. In these cases, the amplitude of a sound is expressed in the unit of decibel (*dB*). Hence, amplitude is also known as the loudness of a vibration in most cases.

Vibration in general is viewed as necessary or unnecessary depending on its purpose for a certain scenario. The delightful sound made by an instrument is viewed as necessary vibration. Meanwhile, the annoying humming sound from a generator is usually viewed as unnecessary vibration. Other than that, study has shown that long term exposure to vibration has various negative effect to a human body. The study is done on 168 workers that expose to vibration regularly with the results of getting pain in fingers, pain in shoulder, pain at the lower back, hearing difficulty and many more occupational diseases. (Issever et al., 2003) However, the vibration caused by moving parts in these mechanical machines are unavoidable. It can be mitigated through the used of damping materials that absorb these vibration.

One of the most popular damping materials used for mitigating vibrations from mechanical machines is rubber pad made with natural rubber. The rubber pad is placed in between the vibrating body and the supporting

surface to mitigate the vibration transferred across the system. In many cases, the dynamic characteristics of the rubber pad are unimportant for consideration as long as it does the job. However in some cases, the dynamic characteristics of the rubber pad are very critical for its effect on a system. The rail pad sandwiched between the train track and the sleeper are one of the few cases that requires precision in the dynamic characteristic of the material that it is made of, which in most of the cases are from natural rubber. That is why rail pad can often be referred to as rail rubber pad too. In order to make sure the precision, the dynamic characteristics of commercially used rail pads should be examined with a test rig.

1.2   Importance of the Study

Rail pad is one of the essential elements in a railway system. The main function of a rail pad on a railway system is to mitigate the vibration transferred to the sleeper where the track is being passed through by the train. By doing so, the rail pad not only protects the railway from wear and tear, and prolongs the service life of the railway system, while also providing a more comfortable riding experience to the passengers. However, these functions can quickly diminish if a railway system is not designed according to the specification of the rail pad. The outcomes of this present study may provide insight for the reader into understanding:

- The effect of the dynamic characteristics of the rubber pad on the particular system it is supporting.
- The effect of a rubber pad in mitigating vibration under different preload conditions.

1.3   Problem Statement

Doshin Rubber Engineering (2020) claims that their rail track isolation products provides "vibration and noise attenuation with low static and dynamic stiffness" on their website. Meanwhile, Kumpulan Jebco (2010) claims that their rail pads "retain low stiffness, high resilience (ability to bounce) and low damping properties" from their website. These two companies are both related in manufacturing rail pads for railways. However, from their claims, there is insufficient information on the dynamic characteristics of the rail pads provided

by them. Many rail pads manufacturers often only provide the range of the dynamic characteristics where they obtained from estimating it from the material's properties they used to create the rail pads. The customers lack equipment or method in justifying the information provided by the manufacturer but to trust them. Hence, the problem statement of the current study is summarised below:

- The information of the dynamic characteristics of rail pads with different geometry features is not provided from the manufacturer.
- The end user lacks the ability to justify the dynamic characteristics of the rail pad provided by the manufacturer.

1.4   Aim and Objectives

The definite aim of this study is to propose a valid method that can determine the dynamic characteristics of rubber pads under different preloads. The specific objectives of this research were to:

- Develop a testing rig that can determine the dynamic stiffness and damping coefficients of rubber pads.
- Determine the dynamic characteristics of rubber pads made with different materials and different geometry properties.
- Determine the effects of different preload to the dynamic characteristics of rubber pads.

1.5   Scope and Limitation of the Study

Rail pads are made of many types of polymer materials with natural rubber being the most common material. However in this study, one of the limitations is that the rubber (rail) pads acquired for analysing are made of ethylene propylene diene monomer (EPDM) rubber and natural rubber which does not cover every material type of rail pad available in the market. Thus the result of this study may not be considered for referencing for the missing material type. Additionally, the effect of rubber pads made with different materials and different geometry properties cannot be determined due to insufficient varieties of test specimens that can be analysed for comparison. Another limitation faced in this study is the use of torque wrench and regular bolts instead of force

sensing bolts to impose preload on the rail pad. The issue in using torque wrench is that the preload in axial force should be converted to torque value and the accuracy of this conversion may be affected by the conditions of the bolts and the environment. In addition, Engineering ToolBox (2018) states that torque wrench has a ± 25 % in accuracy. Furthermore, the results obtained from this study lack persuasion as the results differ from the existing research and there are insufficient similar studies to provide justification for the results of this study.

1.6   Outline of the Report

This body of content of this report is separated into five chapters. The first chapter provides an introduction to the study, where the background of the study alongs with the problem statements, objectives and limitations faced in the study are presented. The second chapter presents a literature review done in advance of embarking into this study. The third chapter provides information regarding the methodology that is adapted and the details of the work plan for this study. The fourth chapter records the results that are obtained from the study and thorough discussions contrary to the results based on the objectives of this study are provided. The last chapter concludes the study directing the results obtained and the objectives that have been achieved in this study, recommendations for further research are also provided.

CHAPTER 2

LITERATURE REVIEW

2.1   Introduction

In this chapter, the literature review begins by introducing the experimental method that was previously developed and will be adopted in this study, which is the instrumented hammer impact test. After that, an introduction to the composition of rubber will be given along with the applications of the damper that is made of rubber material. The next part is devoted to a thorough examination of the study's main topic, rail pads. There are five subsections in this section. The first subsection provides an overview of the railway sector and the importance of rail pads. The second subsection delves into the track's components as well as the various sorts of tracks accessible around the world. The third subsection then goes into studies on the importance of rail pad stiffness in train tracks. The fourth subsection goes into greater detail on the elements that influence rail pad stiffness. Finally, investigations on the effects of geometry on the properties of rubber dampers and rail pads are discussed in the final subsection. After that, the literature review concludes with a brief summary before going on to the next chapter.

2.2   Instrumented Hammer Impact Test

Instrumented hammer impact test was first developed by Kaewunruen and Remennikov (2005) as a method to determine the dynamic properties of a rail track straight from the field based on a two-degree-of-freedom (2DOF) dynamic model of the railway track. The method is then further developed to suit a single-degree-of-freedom (SDOF) system model in determining the dynamic characteristics of a rail pad. Kaewunruen and Remennikov (2008) then used this adaptation to set up an experiment test rig at University of Wollongong to advance in their study away from the field. It is proven from their study that the dynamic stiffness and damping coefficient of every type of rail pad used in Australia when put under different preload conditions, can be acquired with this easy, dependable, quick, and environmentally-friendly method.

In order to obtain the dynamic characteristics of the rail pad, the equation for the frequency response function (FRF) is derived by Kaewunruen and Remennikov (2005). The derivation starts with the equation of motion for the SDOF model in the vertical direction:

$$m_p \ddot{x} + c_p \dot{x} + k_p x = f(t) \tag{2.1}$$

where

m_p = effective rail mass, kg

c_p = damping coefficient of rail pad, Ns/m

k_p = dynamic stiffness of rail pad, N/m

$$\omega_n{}^2 = \frac{k_p}{m_p}, \qquad 2\zeta\omega_n = \frac{c_p}{m_p}, \qquad \zeta = \frac{c_p}{2\sqrt{k_p m_p}} \tag{2.2a, b, c}$$

where

ω_n = natural frequency of rail pads, rad/s

ζ = damping ratio

The magnitude of FRF is then determined with the Fourier transformation of equation (2.1) which gives the following:

$$H(\omega) = \frac{1/m_p}{\sqrt{(\omega_n{}^2 - \omega^2)^2 + (2\zeta\omega\omega_n)^2}} \tag{2.3}$$

The magnitude of the FRF $H(f)$ is then derived by substituting equation (2.2) into equation (2.3) and using $\omega = 2\pi f$ which is shown as following:

$$H(f) = \frac{1}{m_p} \frac{4\pi^2 \beta f^2}{\sqrt{[1 - 4\pi^2 \beta f^2]^2 + \left[4\pi^2 \beta \left(\frac{c_p{}^2}{k_p m_p}\right) f^2\right]}} \tag{2.4}$$

where

$$\beta = \frac{m_p}{k_p} \qquad\qquad (2.5)$$

The m_p, c_p, and k_p components evaluated from equation (2.4) are used for the curve-fitting parameters.

2.3 Rail Pads

2.3.1 Railways

Prebuilt railways in rail transport are used by wheeled vehicles in transferring merchandise, goods, or passengers between locations. (Sol-Sánchez et al., 2015). The steel I-beam used in construction of a pair of rails will guide and support the train as it drives forward on the track. The train's weight, as the train travels, generates a dynamic loading directly onto the rails below the train wheels, which can induce track vibration and produce noise. Excessive track vibration can result in the cracking of concrete sleepers that underlies the rails, whereas the noise produced will also become a nuisance to residents nearby. (Sol-Sánchez et al., 2015). Hence, rubber rail pads are applied as a rubber damper to the track to damp the vibration incurred by moving trains and also serving as electrical insulation between the track rails (Sol-Sánchez et al., 2015).

2.3.2 Rail Tracks and Rail Pads

During the rail installation, in order to fasten the rail against the sleeper, rail clips are included to exert a clamping force onto the rail foot. Whereas rail pad is placed below the rail to create a soft layer between the rail and sleeper that dissipates vibration.

There are mainly two types of tracks, the ballasted track and the slab track. Ballasted track is a multi-layered substructure forming the foundation of the track. It contains the ballast, sub-ballast, and subgrade layers. The ballast layer, which consists of free-draining, coarse granular material, underlies the sleeper to transfer dynamic loads generated from the train to the sub-ballast and subgrade layers below (Indraratna et al., 2017). Whereas for slab track, a flat concrete slab is built to support the track instead of a ballast layer, followed by

cement asphalt mortar (CAM) and concrete supporting layers underneath. An isolation layer laid with rubber pad is sometimes included between the CAM and supporting layers to suit the application of high speed heavy trains (He et al., 2018).

2.3.3 Railway Overall Stiffness

One of the most crucial parameters for the railway track is the overall stiffness. Research has shown that the fastener stiffness and elastic modulus of the substructure will influence the dynamic displacement of track-subgrade system with high elastic modulus of the substructure results in smaller vibrational displacement of the embankment and subgrade layers (Chen and Zhou, 2020). The force generated at the interface between the train wheel and rail is determined by the stiffness gradient at the transition zone between the fixed and floating slab tracks; this factor is important as gradual change throughout the transition zone is necessary to reduce the wheel/rail impact as compared to an abrupt jump in stiffness (Xin et al., 2020). As a softer rubber pad stiffness dominates the total vertical stiffness of slab track, the addition of rubber pad between the supporting layer and concrete slab in slab track was discovered to significantly attenuate vibration transferred to the supporting layers (He et al., 2018).

Evidently, these authors demonstrate that the vertical stiffness of track determines the dynamic response of the track components. Thus, the rail pad needs to have the appropriate stiffness to mitigate the track stiffness, in order to reduce vibration and to achieve desirable track response.

2.3.4 Aspects Affecting Rail Pad Stiffness

Existing studies have shown that temperature is a crucial factor affecting rail pad stiffness. Wei et al. (2016) investigated the temperature effect on rail pad stiffness of CR, TPE, and EPDM rail pads, and has found that the static stiffness for the three rail pads is non-linear with temperature changes. In the low temperature range (-40 – 20 °C), the stiffness drops greatly. Whereas in high temperature range (20 – 70 °C), it is relatively stable, except for TPE pad which shows an abrupt jump in stiffness at 60 °C. Hence it becomes particularly

problematic for railroad in seasonal countries as the rubber becomes too stiff in winter for effective vibration damping.

Moreover, frequency also influences the rail pad stiffness. Different types of train travel at different speeds on the rail track, resulting in different frequency at which the train weight imposes on the rail pad. Wei et al. (2017) looked into the dependency of rail pad's dynamic characteristics on temperature and frequency for rail pads used in various fastening systems. Both storage modulus and loss factor of rail pad are found to increase gradually with the dynamic load frequency. They also noted that the storage modulus shares a similar trend of temperature dependency of rail pad stiffness as observed in Wei et al. (2016), in which the loss factor of rail pad rises with temperature until it peaks at the glass transition temperature of rubber before dropping with temperature.

Figure 2.1 shows a table from the paper by Köse (2015) stating the effect of different temperatures on the static stiffness of different rail pads and the effect of changing load frequencies on the dynamic stiffness of different rail pads. From the table, it can be observed that the static stiffness of rail pads increased when the temperature increased. Meanwhile, the dynamic stiffness of the rail pads increased when the loading frequency increased.

Çizelge 2.3 : Bazı ray elastik tabakalarının statik ve dinamik yay katsayıları (Öztürk ve Arlı, 2009).

	Statik Rijitlik (MN/m)			Dinamik Rijitlik (MN/m)	
	-30°C	25°C	70°C	25°C, 5-30 Hz	25°C, 100-2000 Hz
Zwp104NT*	22	23	25	28-29	-
Zwp104	26	27	29	40-42	-
Zw1000NT	42	42	41	57-61	-
Zw700a	51	53	64	71-77	80-275
Zw900a	53	56	68	75-83	-

*Zwp: Zwischenplatte (Bağlantı plakası)

Figure 2.1: Table from Köse (2015)

Interestingly, the dynamic loading amplitude also found to be altering rail pad stiffness. Wei et al. (2016) have investigated the influence of dynamic amplitude on the rail pad stiffness. They found that increasing load amplitude

can result in stiffening of the rail pad. They also concluded that amplitude and frequency dependencies are important to be considered when predicting railway pad stiffness, as compared to secant stiffness or frequency-dependent stiffness as both underestimate the random vibration levels at high frequency range of 65 – 150 Hz.

During function, the clamping force from the rail fasteners on the rail pads, also known as toe load, translates to static preloading on the rail pad. Kaewunruen and Remennikov (2008) found that the dynamic stiffness of studded rubber rail pad increases with the preload level. At low preload level, the dynamic stiffness increases substantially, but reduces in increments as preload increases further.

Lastly, Sainz-Aja et al. (2020) have investigated all the factors previously mentioned on EPDM, TPE, and EVA rail pads. Their findings basically agree with those discussed above, where the rail pad stiffness generally increases when temperature reduces, load increases, or excitation frequency increases.

In summary, rail pad stiffness is influenced by multiple factors as mentioned above, due to rubber's intrinsic characteristics to be capable of being influenced by temperature, dynamic load frequency and amplitude, and preloading. This is relevant to all rubber dampers and not just exclusively rail pads.

2.3.5   Effects of Geometry Properties on Rubber Pad

It is widely acknowledged that the geometry of rubber dampers or isolators affects their dynamic performance during vibration. Hence, studies have been carried out to study the impact of different geometry alteration to rubber damper properties to gain insight into ways of optimising existing rubber damper design. An example of geometrical impact on rubber isolator was demonstrated by Ali et al. (2017), who found that the rubber with hexagon shape produces the lowest deformation and stress intensity as compared to trapezoidal and cylindrical shapes during static and dynamic loadings, concluding that the hexagonal shape is the most suitable among the three shapes for extending operational period of the rubber damper.

Li et al. (2011) introduced 14 holes into the rubber material of an equipment rubber isolator used for isolating machines on ships. When compared to those without holes, their simulation has shown that the introduction of hole features into the isolator reduces the resonant vibration amplitude of the steel plane (floor) by 3.4 dB under excitation force of 10 N.

In railway's studies, using finite element analysis, Ouyang et al. (2015) studied the various geometrical parameters, including the height, width, and inclined angle, of the rubber damper used in shear-type rail fastening system (Cologne Egg) to damp vibration caused by moving train. They found that the vertical stiffness of the rubber is softened significantly by increasing thickness of rubber width. This is because the large width allows the free surface to grow during shearing deformation from excitation. On the other hand, the increase of rubber height and inclined angle is found to increase the vertical stiffness of the fastening system.

Zakeri et al. (2021) introduced the placement of a rubber sheet in the soil bed of the machine foundation to achieve better dynamic response during machine vibration. They also investigated the influence of rubber sheet thickness in improving the dynamic performance. They found that by applying a 6 mm rubber sheet and increasing the thickness up to 24 mm, the foundation's resonant frequency and equivalent shear modulus decreased by 22% and 36% respectively, indicating that increased sheet thickness lowers the dynamic stiffness of rubber sheet so that it alters the total stiffness of the soil bed.

Furthermore, Sol-Sanchez et al. (2014) found that rail pad stiffnesses rise with reducing thickness, where the stiffness increases even more prominently for rail pads with thickness less than 6 mm. It was also shown that the relation between both the stiffnesses and thickness can be related by a power law model.

Rail pads come with many features, such as grooves and studs on pad surfaces. These rail pad designs are widely used around the world. However, there is limited literature focusing on the influence of such features on rail pad stiffness as well as investigation on possible features that can be introduced into the rail pad design to optimise it.

2.4   Summary

In a nutshell, the instrumented hammer impact test that this study is going to be adopting has been introduced in this literature review. The method is proven to be reliable in obtaining the dynamic characteristics of a rail pad under different preload conditions. Then, the basic knowledge of rubber was discussed. Different hyper-elastic and viscoelastic constitutive models have been created to describe their behaviour because of their inherent non-linear stress-strain behaviour and viscous damping effect. Rubber is used in a variety of vibration damper applications because of these qualities. Rail pads, for example, are used in railways to reduce excessive track vibration. Various studies have inferred that one of the most essential properties of rail pads is their stiffness, which allows them to reduce overall track stiffness and generate a desired track dynamic response. As a result, research was conducted to determine the effect of geometry properties on rail pad stiffness. However, because the thickness of rail pads was emphasised as the primary element in altering stiffness, other geometrical aspects such as grooves and studs were overlooked. Furthermore, no research has been done to look at additional geometrical elements that could be added to rail pads to influence their stiffness.

Hence, an experimental test rig adopting the instrumented hammer impact test will be set up to analyse the dynamic characteristics of the rubber pads under different preload conditions. Rubber pads with different geometry properties will be studied for the impact on their respective dynamic characteristics.

CHAPTER 3

METHODOLOGY AND WORK PLAN

3.1   Introduction

In this chapter, the methodology adapted in this study will be discussed and the work plan of the project will be outlined. This study involved two experiments in which one of the experiment requires a setup be designed and test specimens will be identified and analysed in both experiments under different conditions. This chapter includes six subsections. First subsection descripts the two experiments that will be conducted and the experiment setup requires to be designed according to a test rig developed in a previous study. Second subsection introduces the equipment and materials required for both experiments in this study. Then, the third subsection dives into the test specimens identified for analysing their dynamic characteristics in this study. The fourth subsection describes the experiment procedures that has been planned out. Moving on, the preload conditions that will be imposed on the test specimens is discussed and computed in the fifth subsection. Lastly, the overall work flow of the project will be shown in the sixth subsection with a flow chart.

3.2   Experiments Setup and Description

Figure 3.1 shows the experiment setup for the first experiment that analyses the dynamic characteristics of the rubber (rail) pads. This setup utilised the instrumented hammer impact test method that is based on a base-isolated test rig that has been developed at the University of Wollongong by Kaewunruen and Remennikov (2008). The setup consists of a concrete block, the steel plate then glued to the top of the block with bonding glue. The rubber pad is then placed on top of the steel plate followed by the preloading bolt system. Regular hex bolts are used instead of force sensing bolts from the original test rig because of unavailability. The hex bolts will be torque down to specific preload with a torque wrench to replicate the preload conditions. An accelerometer is secure on the centre of the top of the steel upper block. Every component is placed in a centre aligned manner when setting up the experiment. Figure 3.2 shows the instrumented hammer impact experiment setup assembled together.
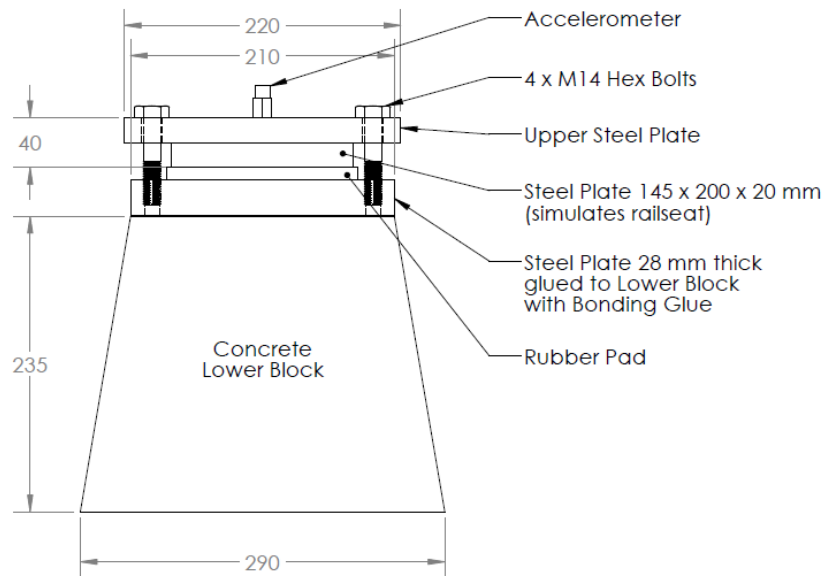
Figure 3.1: Schematic Diagram of Instrumented Hammer Impact Experiment Setup

Figure 3.2: Instrumented Hammer Impact Experiemnt Setup

The second experiment analyses the static stiffness of the rubber pads under different compression loads by using the compression test method with a universal testing machine. The rubber pad is compressed with the bottom surface fully covered and the top surface covered with the same manner as in the instrumented hammer impact experiment by using the same steel plate (railseat). The rubber pads will be compressed with a fixed strain rate until the detected compression load reaches the predetermined maximum load. The setup for this experiment is shown in Figure 3.3.
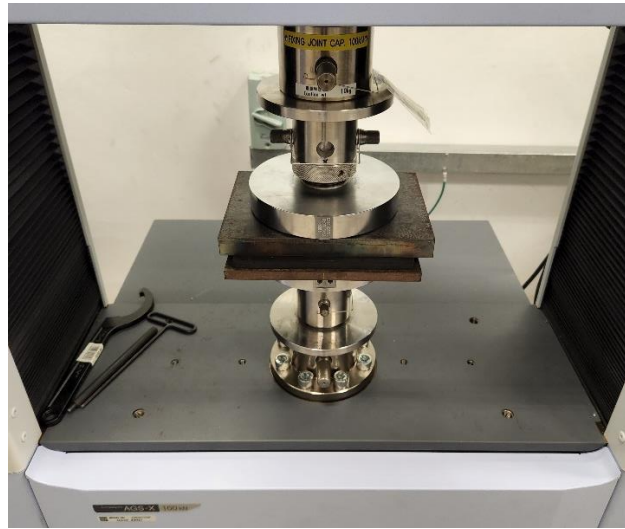
Figure 3.3: Compression Test Experiment Setup

3.3   Equipment and Materials

Table 3.1 shows the equipment and materials that will be used in both experiments alongside with the experiment setup to obtain the data requires to compute the dynamic characteristics and the static stiffness of the rubber pads. For the first experiment, the impact hammer is used to induce an impact force on the upper steel plate. The resulting FRF will then be picked up by the accelerometer sat on top of the upper steel plate along with the help of IMC Software from the connected computer. The data will then be analysed with ME'scope software.

Table 3.1: Equipment and Materials

Item Description	Item Category	Quantity
IMC Cronos-PL	Equipment	1 set
Triaxial Accelerometer	Equipment	1 set
Impact Hammer	Equipment	1 set
Torque Wrench	Equipment	1 set
Shimadzu AGS-X 100 kN	Equipment	1 set
Computer	Equipment	1 unit
IMC Software (Bundle of Studio 5, Wave and Famos)	Software	1 licence
ME'scope	Software	1 licence
TRAPEZIUM X	Software	1 licence
Microsoft Office	Software	1 licence

For the second experiment, the universal testing machine (Shimadzu AGS-X 100 kN) is used to compress the rubber pad to a preset compression load with a constant strain rate. The data are recorded with the help of TRAPEZIUM X software and the static stiffness of the rubber pads at the desired compression load can be computed using Microsoft Excel's graph function.

3.4   Test Specimens

The test specimens to be analysed for their dynamic characteristics in this study are a rail pad that is provided from a European manufacturer and also rubber pads that are bought with the dimension of a standard rail pad. The materials that made up the rubber pads used for this study are EPDM and natural rubber. A total of three rubber pads are used in this study that have a general dimension according to the standard dimension for rail pads that are studied by Oregui et al. (2016) which is 152 mm × 152 mm × 4.5 mm but with the thickness change to 10 mm instead of 4.5 mm. This allows room for different geometry properties to be introduced to the rubber pads for testing. The rubber pads used in this study are shown in Figure 3.4. From left to right, the first rubber pad is a railpad made with EPDM provided by the manufacturer, the railpad is specified as Zw1000NT and rated with a static stiffness of 35 MN/m ±15 %. The second one is a store bought EPDM rubber pad. The third one is a rubber pad made with natural rubber with 3 mm × 3 mm grooves on both sides.
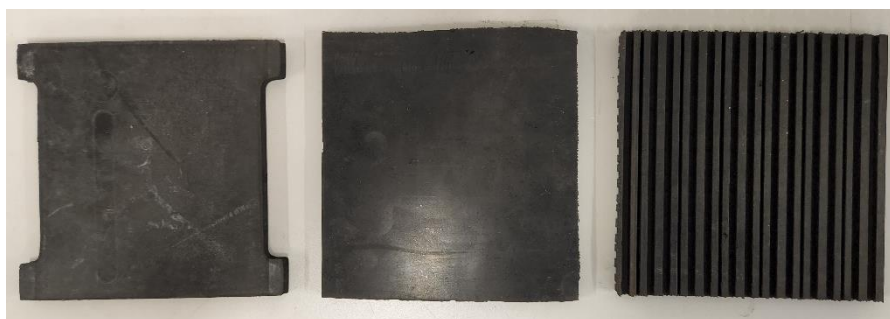

Figure 3.4: Rubber Pads used in this Study

3.5   Experiment Procedures

The experiments can proceed after the test rig is set up and the test specimens are identified. For the instrumented hammer impact experiment, first step is to make sure the accelerometer and the impact hammer are connected to the

selected channel on the IMC Cronos-PL. Place the rubber pad on the right spot before putting on the preloading bolt system. Then, torque down the bolts with the torque wrench to the specific preload amount. Since the force sensing bolts are not available, the amount of torque for the bolts should be computed from the specific preload with the following equation (Engineering ToolBox, 2018):

$$\tau = K \times F \times d \times \left(1 - \frac{l}{100}\right)$$ (3.1)

where

τ = wrench torque, Nm

K = constant that depends on the bolt material and size

F = axial bolt force, N

d = nominal bolt diameter, m

l = lubrication factor, %

The bolts are assumed to be in normal dry condition ($K = 0.2$) and no lubricant are used on the bolts ($l = 0$ %). The experiment proceeds by striking the top of the upper block 10 times with the impact hammer to obtain the coherence function to evaluate the quality of FRF measurements (Kaewunruen and Remennikov, 2008). After that, repeat the experiment with the same rubber pad at different preload settings and then with different rubber pads at different preload settings.

For the compression test experiment, setup the experiment by placing the rubber pad and the steel plates on the universal testing machine as shown in Figure 3.2, the steel plate (railseat) should cover in the rubber pad in the same manner as in the instrumented hammer impact experiment as the data obtain will be use for comparison and justification for the results from both experiments. With the TRAPEZIUM X software, fix the strain rate to 5 mm/min and the maximum compression load of 60 kN. Initiate the compression test for each rubber pad separately to obtain the stress–strain graph for each rubber pad. Make sure to exercise the precautions of operating the universal testing machine at all times when doing the experiment.

3.6 Preload Conditions

According to Kaewunruen and Remennikov (2008), the average preload exerted on a rail pad by a Pandrol e-Clip fastening system is about 20 kN. Hence, a range of preloads that are close to 20 kN should be tested on the rail pads. In this study, the preload applied to the rail pad by the hex bolts will start at 10 kN and increase with an interval of 10 kN until 50 kN. As previously discussed that force sensing bolts are unavailable, the preload (axial load) exerted by the bolts should be converted to torque in order to be referred to when using a torque wrench. The converted torque values are calculated with equation (3.1) and shown in Table 3.2. The bolts are torqueed down in a criss-cross manner in order to equalise the torque of each bolt.

Table 3.2: Preload Amount and Converted Torque Values

Preload Amount, kN	Converted Torque Value, Nm
10	28
20	56
30	84
40	112
50	140

3.7 Work Plan

To make sure the project can progress in an organised fashion, a flow chart of the project workflow is planned as shown in Figure 3.4. The project initiates with reviewing the previously done researches that are related to this study to gather information for the literature review section. Next, with enough information, the importance of study, problem statement, aim and objectives, and scope and limitations of this study can be determined. After that, the test specimens that will be used for analysing their dynamic characteristics and static stiffness will be identified. Simultaneously, the preload conditions to induce on the test specimens will be selected. Then, the experiment setup will be designed according to previous study and the experiment's procedures will be planned out.

After all of that has been done, the experiment test rig for the instrumented hammer impact experiment can be set up. The project can now proceed into conducting the experiments on each test specimen. The FRFs from

different test specimens under different preloads will be logged with IMC Software and evaluated for their dynamic characteristics with ME'scope software. The stress–strain graph of each test will be logged with TRAPEZIUM X software and evaluated for their static stiffness at the desired compression load using Microsoft Excel's graph function. The experiments are completed when both experiments have been done for all of the test specimens with different preset conditions. Afterwards, the project moves to compiling results and forming discussion before ending with a general conclusion on the study.
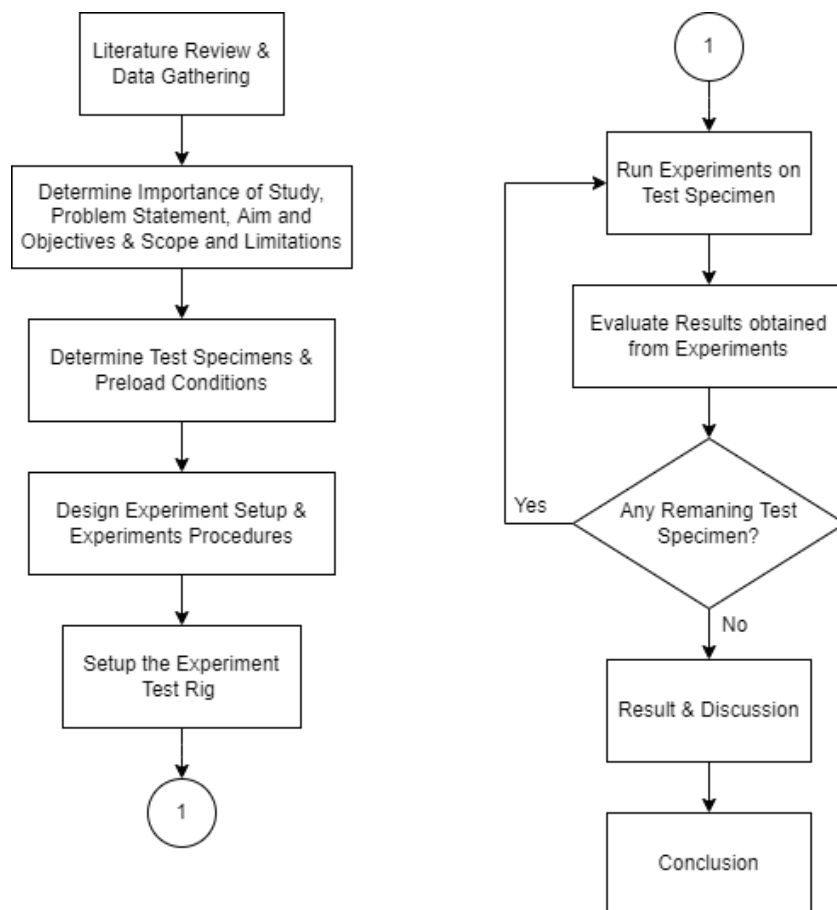
Figure 3.4: Flow Chart of Project Work Flow

CHAPTER 4

RESULTS AND DISCUSSIONS

4.1 Introduction

In this chapter, the results obtained from the experiments done on the test specimens and the results of analysing the steel plates with the instrumented hammer impact test method will be shown. All of the results shown will be followed with discussions that provide insight of the method used to obtain each result and interpretation of the contribution of each result in achieving the objectives of this study. References of relevance sources will be included if possible in order to support the results obtained and further justify their reliability and authenticity. This chapter is preceded by showing the results obtained with an instrumented hammer impact test on the steel plates that will be used in justifying the reliability of the experiment setup. Next, the results of the compression test experiment on the test specimens will be shown alongside with the computation of the static stiffness of the rubber pads and how these results will be beneficial later on in the study. Lastly, the results of the instrumented hammer impact experiment on the test specimens will be shown and followed with the computation of the dynamic stiffness and damping coefficient of the rubber pads under different preload conditions. The computed static stiffness of the rubber pads will be used as comparison the further verify the authenticity of the results obtained from the experiment setup.

4.2 Justification of Experiment Setup

In order to measure the vibration response of the rubber pads accurately, the vibration response other than coming from the rubber pads must be proven to not interfere or be insignificant when the FRF logged is evaluated. This is possible if the frequency response of the rubber pads are much higher relative to the setup. Thus, the natural frequency of each steel plate must be identified using an instrumented hammer impact method. Figure 4.1, Figure 4.2 and Figure 4.3 show the FRFs and the natural frequencies for the bottom steel plate, steel plate (railseat) and top steel plate respectively.
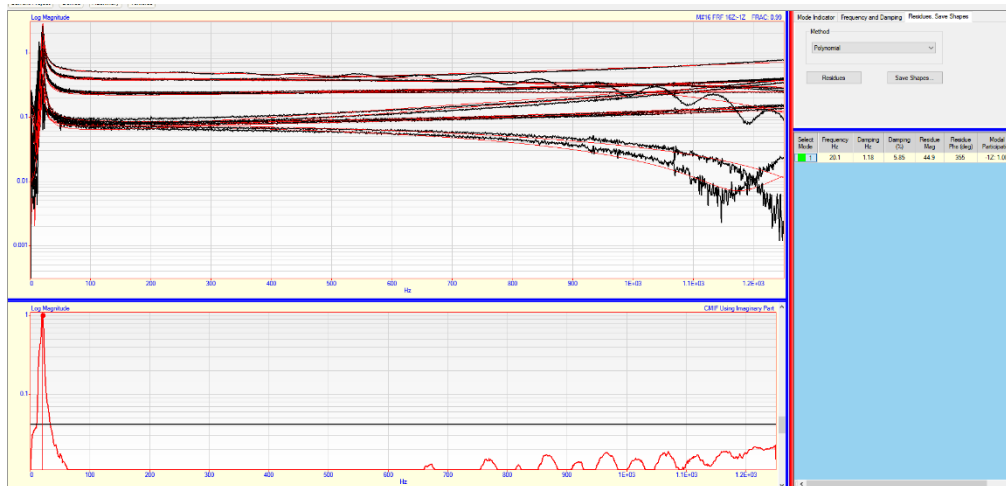
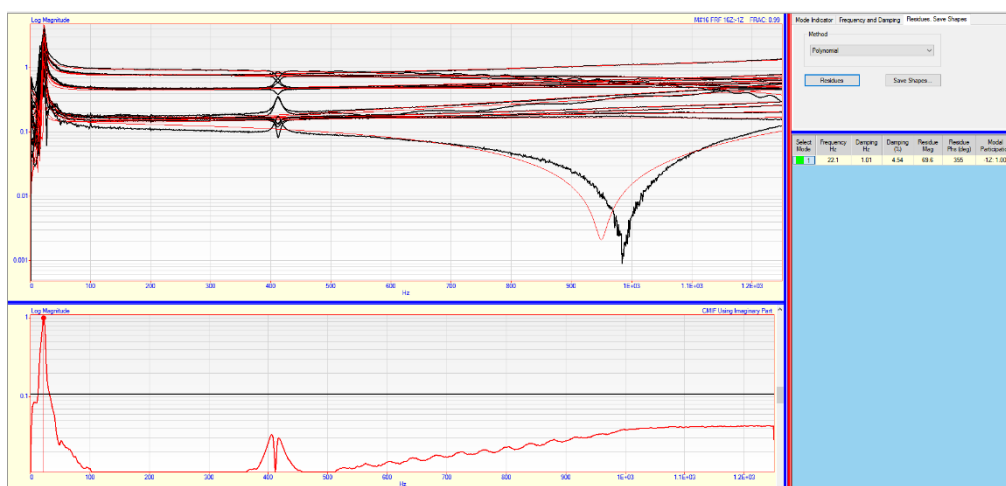Figure 4.1: FRF and Natural Frequency of Bottom Steel Plate

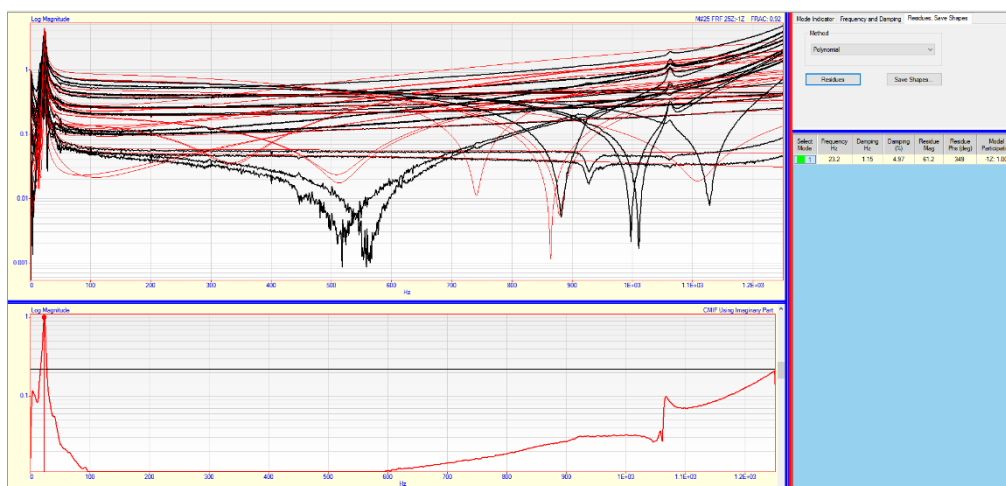Figure 4.2: FRF and Natural Frequency of Steel Plate (Railseat)

Figure 4.3: FRF and Natural Frequency of Top Steel Plate

The natural frequencies of the rubber pads are computed with the curve-fitting function from the ME'scope software. Notice from the FRF curves of three steel plates all having the similarity of having one pronounced peak. This is because the testing method used on the steel plates resembles the system as a SDOF system. Thus, only the natural frequency of the first mode of vibration is detected in this case. Table 4.1 shows the natural frequency of each steel plate obtained. Among the three steel plates, the top steel plate has the highest measured natural frequency of 23.2 Hz while the bottom steel plate has the lowest measured natural frequency of 20.1 Hz. However, it can be said that the three steel plates have relatively similar natural frequency which is around 22 Hz. When comparing this result with the result obtained from the instrumented hammer impact experiment on the test specimens, Table 4.3 shows that the EPDM railpad has the lowest natural frequency of 897 Hz amongst the three rubber pads at the preload of 10 kN, which is significantly higher than the general frequency of the steel plates which is 22 Hz. Thus, it is safe to say that the vibration response of the steel plates will not interfere with the results from the instrumented hammer impact experiment.

Table 4.1: Natural Frequency of each Steel Plate

Steel Plate	Frequency (Hz)
Bottom Plate	20.1
Railseat	22.1
Top Plate	23.2

To further verify the reliability of the experiment setup, the test rig is bonded rigidly to an isolated platform, which is shown in Figure 3.1 where the test rig has its bottom steel plate glued statically to the heavy concrete block. Note that the concrete block is placed on four identical rubber pads at each corner to further isolate the whole setup from surrounding ground vibration. This has essentially made the whole experiment setup into a SDOF system. This proves to be beneficial as the instrumented hammer impact experiment will only detect the first mode of vibration of the rubber pads and the dynamic properties can be calculated with the equation of motion (EQM) formula of a SDOF system.

4.3   Static Stiffness of Rubber Pads

The results shown in this subsection are obtained from the compression test experiment done on the test specimens. Figure 4.4, Figure 4.5 and Figure 4.6 shows the graphs of the compression of EPDM railpad, store bought EPDM and natural rubber pad from 0 kN to 60 kN of compression load at a fixed strain rate of 5 mm/min respectively. From the three graphs, it can be observed that the load increases when the compression of the rubber pads increases. The static stiffness of the rubber pads at a certain load can be found by computing the gradient of the respective graph at the certain load.
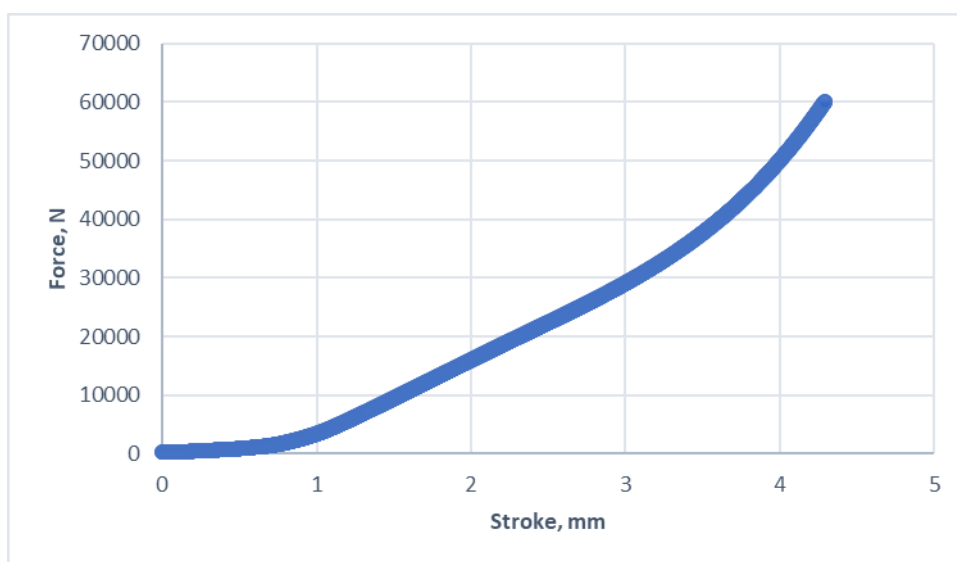
Figure 4.4: Compression of EPDM Railpad from 0 kN to 60 kN Load
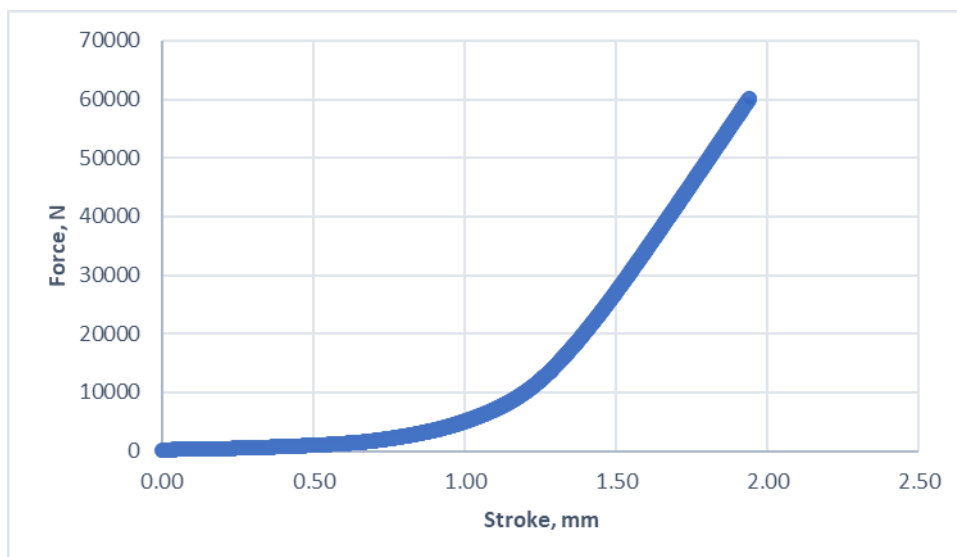
Figure 4.5: Compression of Store Bought EPDM from 0 kN to 60 kN Load
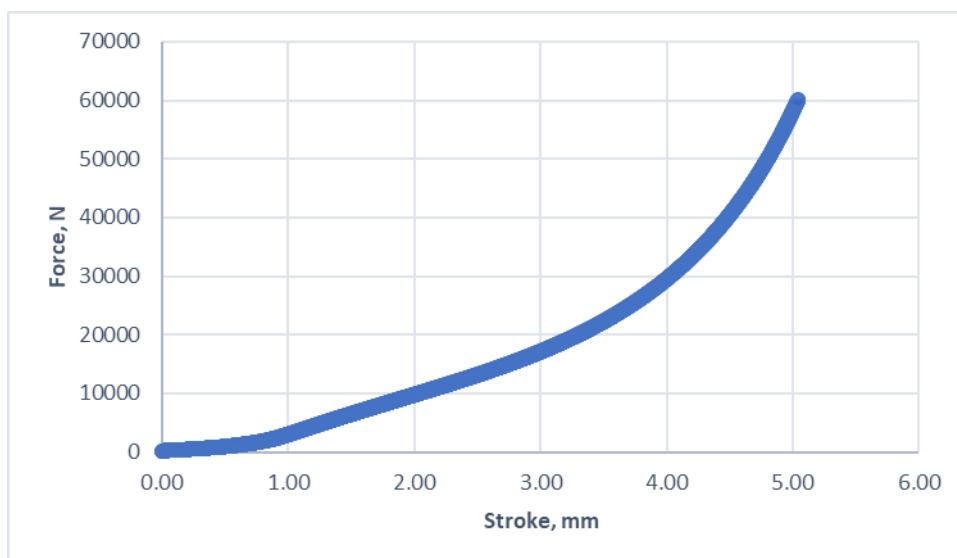
Figure 4.6: Compression of Natural Rubber Pad from 0 kN to 60 kN Load

Figure 4.7 shows an example of finding the static stiffness of EPDM railpad at 50 kN of load. This is done by applying the trendline function from Microsoft Excel to the data of EPDM railpad compressed with 49 kN to 51 kN of load. The gradient of the equation of the trendline is equal to the static stiffness of the EPDM railpad at the middle of the range of data, which is 50 kN of load. From the gradient obtained, the static stiffness of EPDM railpad at 50 kN of compression load is equal to 30.381 MN/m, which is relatively close to the rated static stiffness of 35 MN/m ±15 % by the manufacturer.
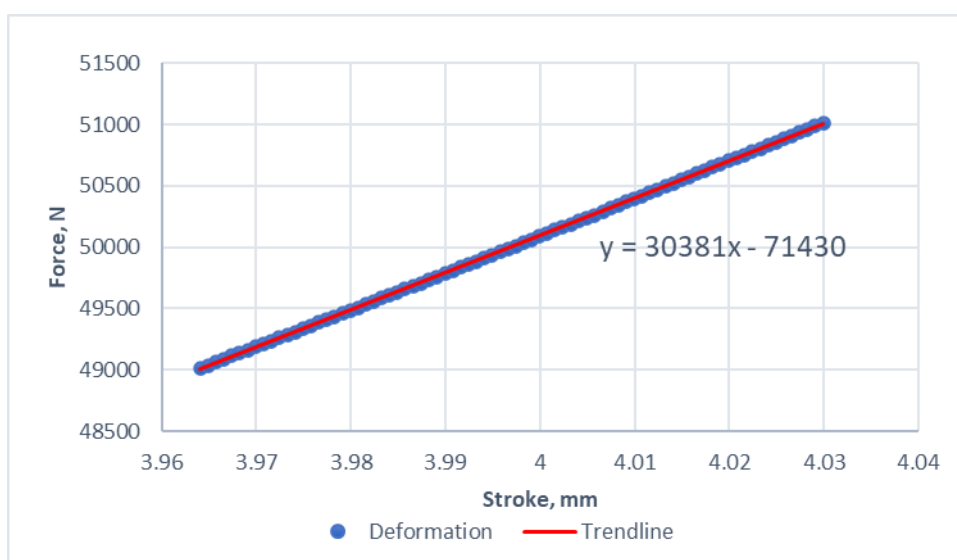
Figure 4.7: Compression of EPDM railpad from 49 kN to 51 kN Load

By using the same method, the static stiffness of other two rubber pads at 50 kN of compression load can be obtained. Table 4.2 shows the static stiffness of three rubber pads at 50 kN of compression load. Among the three rubber pads, store bought EPDM has the highest static stiffness which is 76.217 MN/m, natural rubber pad is significantly softer than store bought EPDM and slightly stiffer than EPDM railpad with a static stiffness of 36.819 MN/m, EPDM railpad is the softest with a static stiffness of 30.381 MN/m.

Table 4.2: Static Stiffness of Rubber Pads at 50 kN of Compression Load

Rubber Pad	Static Stiffness (MN/m)
EPDM Railpad	30.381
Store Bought EPDM	76.217
Natural Rubber Pad	36.819

However, according to the table shown in Figure 2.1, Köse (2015) claimed that Zw1000NT railpad has a static stiffness of around 42 MN/m, which is higher than the static stiffness of the EPDM railpad used in this study, which is rated at 35 MN/m ±15 % by the manufacturer. This shows that although both railpads are specified as Zw1000NT, the static stiffness can be different when the railpad is produced by different manufacturers.

From the results, it can be noted that the store bought EPDM is stiffer than the EPDM railpad despite they both having the same general dimension and made with the same material. To explain this, the store bought EPDM must have a higher density than the EPDM railpad with the same volume. Wang et al. (2010) claims that the stiffness of metal rubber damper increases when the relative density increases.

4.4   Dynamic Properties of Rubber Pads

The results shown in this subsection are obtained from the instrumented hammer impact experiment done on the test specimens. As an example, Figure 4.8 shows the FRF of the EPDM railpad preloaded with 10 kN of force with the test rig. The FRF is computed by the IMC Software in the preset frequency range from 0 to 10 kHz. In the process of striking the top steel plate 10 times with the impact hammer, the conference value (red line) is maintained close to one by striking

the same point with approximately the same force for the 10 strikes. The natural frequency of the first mode of vibration of the EPDM railpad is recorded by measuring the frequency of the first pronounced peak from the FRF, which is 897 Hz. This process is repeated for all three rubber pads with all the preload conditions. The natural frequency of each rubber pad under each preload condition is recorded and shown in Table 4.3 and Figure 4.9.
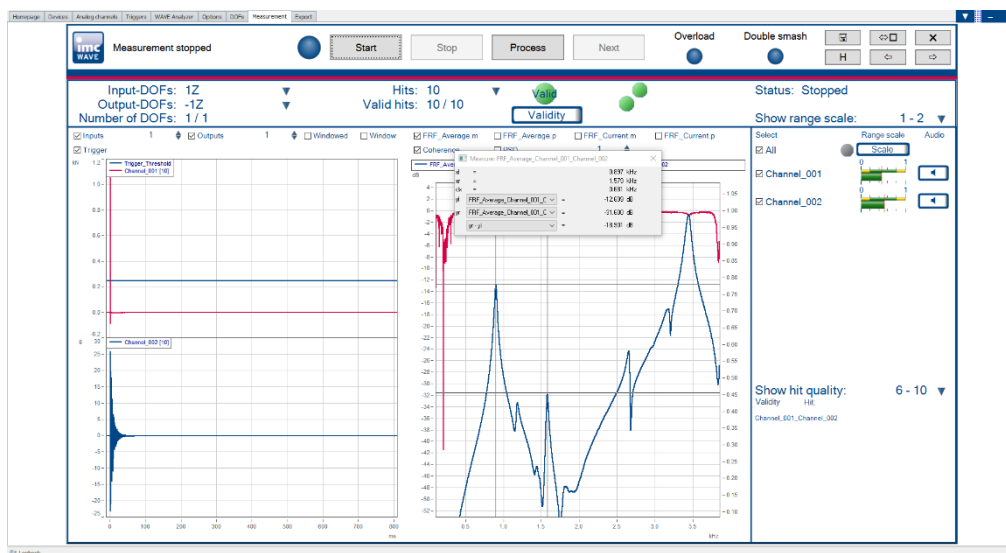

Figure 4.8: FRF of EPDM Railpad under 10 kN Preload by IMC Software

Table 4.3: Natural Frequency of Rubber Pads under Different Preload

Preload (kN)	Frequency (Hz)		
	EPDM Railpad	Store Bought EPDM	Natural Rubber Pad
10	897	1391	1155
20	1069	1410	1334
30	1145	1422	1388
40	1263	1424	1408
50	1339	1425	1424
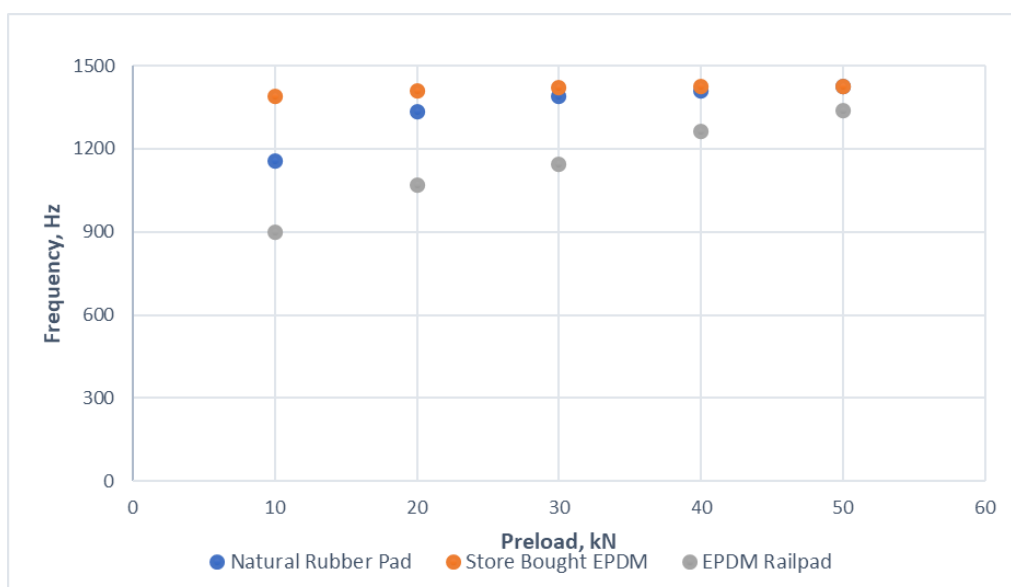
Figure 4.9: Natural Frequency of Rubber Pads under Different Preload

Table 4.4 shows the mass of each steel plate measured. The effective mass experienced by the rubber pad during the experiment is the sum of mass of railseat and top plate, which is equal to 11.859 kg. Using equation 2.2a along with the effective mass and the respective natural frequency, the dynamic stiffness of each rubber pad at different preloads can be calculated. The results are recorded and shown in Table 4.5 and Figure 4.10.

Table 4.4: Mass of Individual Steel Plate

Steel Plate	Mass (kg)
Bottom Plate	9.518
Railseat	4.510
Top Plate	7.349

Table 4.5: Dynamic Stiffness of Rubber Pads under Different Preload

| Preload (kN) | Dynamic Stiffness (MN/m) | | |
	EPDM Railpad	Store Bought EPDM	Natural Rubber Pad
10	376.8	906.1	624.7
20	535.1	931.0	833.3
30	613.9	946.9	902.2
40	747.0	949.6	928.3
50	839.6	950.9	949.6
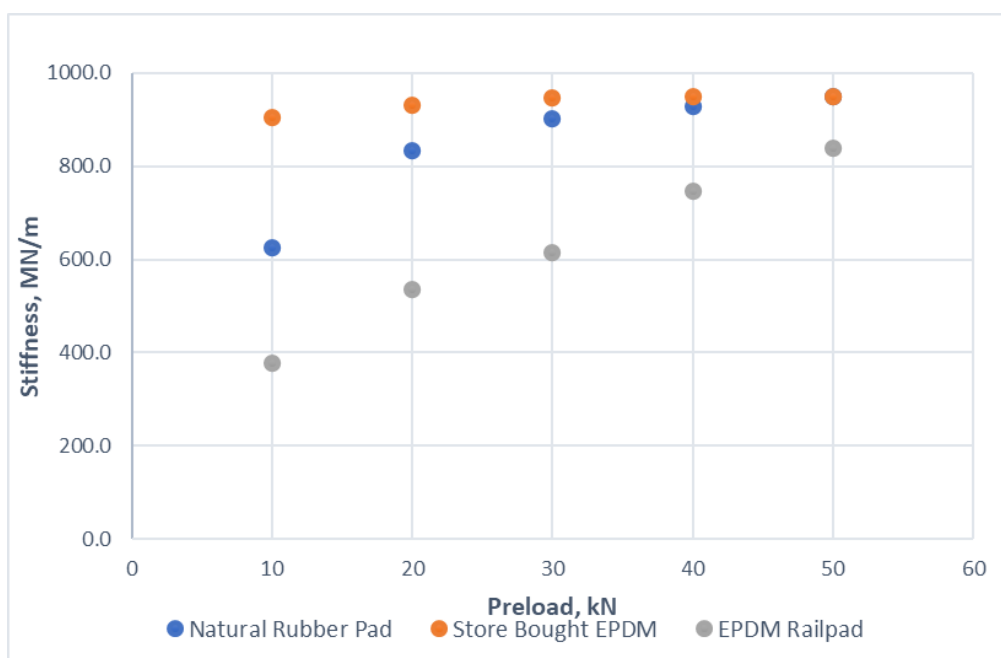
Figure 4.10: Dynamic Stiffness of Rubber Pads under Different Preload

The data logged with IMC Software are then transferred to ME'scope software to be analysed. As an example, Figure 4.11 shows the FRF and the damping ratio computed for the EPDM railpad preloaded with 10 kN of force with the test rig by using the curve-fitting function from ME'scope software. This process is repeated for all three rubber pads with all the preload conditions. The damping ratio of each rubber pad under each preload condition is recorded and shown in Table 4.6. The damping coefficient of each rubber pad at different preloads can be calculated by using equation 2.2c with the effective mass and the respective dynamic stiffness and damping ratio. The results are recorded and shown in Table 4.7 and Figure 4.12.
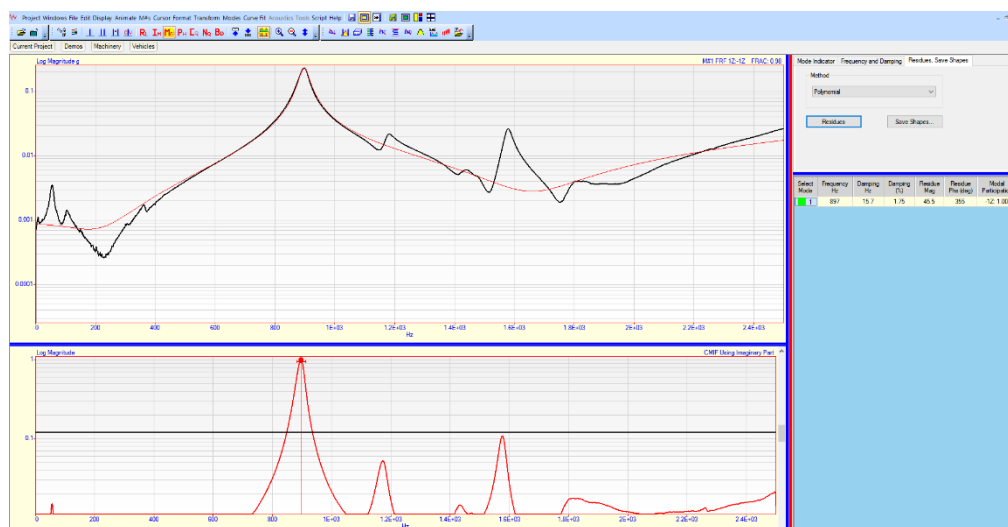
Figure 4.11: FRF and Damping Ratio of EPDM Railpad at 10 kN Preload

Table 4.6: Damping Ratio of Rubber Pads under Different Preload

Preload (kN)	Damping Ratio, ζ		
	EPDM Railpad	Store Bought EPDM	Natural Rubber Pad
10	0.0175	0.0210	0.0399
20	0.0228	0.0062	0.0280
30	0.0249	0.0136	0.0200
40	0.0248	0.0158	0.0105
50	0.0211	0.0138	0.0081

Table 4.7: Damping Coefficient of Rubber Pads under Different Preload

Preload (kN)	Damping Coefficient (Ns/m)		
	EPDM Railpad	Store Bought EPDM	Natural Rubber Pad
10	2340	4354	6868
20	3633	1305	5567
30	4249	2882	4137
40	4668	3353	2203
50	4211	2931	1719
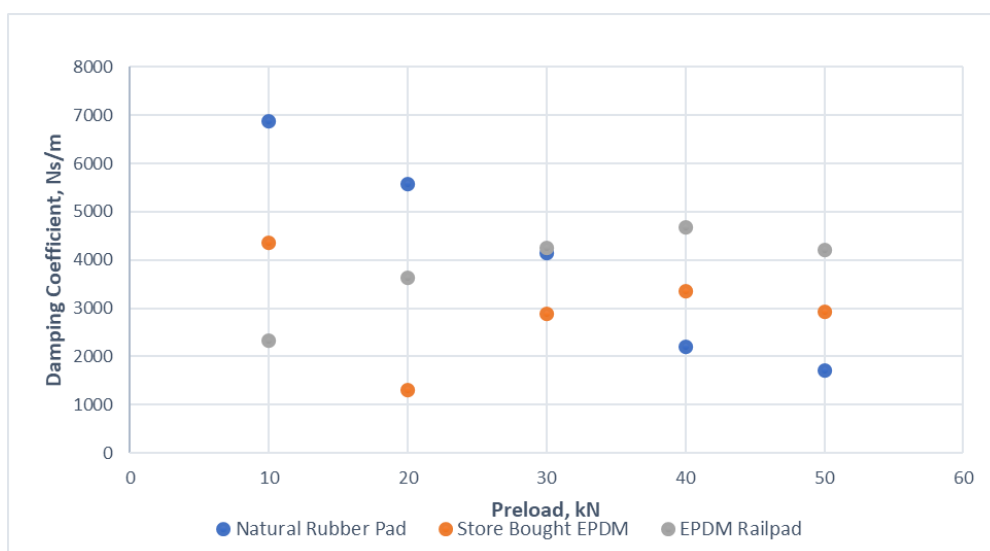
Figure 4.12: Damping Coefficient of Rubber Pads under Different Preload

Based on the results, among the three rubber pads, the store bought EPDM has the highest natural frequencies and dynamic stiffnesses throughout all the preload conditions, the natural rubber pad came second highest while the EPDM railpad came last in terms of the natural frequencies and dynamic stiffnesses throughout all the preload conditions. These results are agreeable when comparing them with the results obtained from the compression test experiment where the store bought EPDM is the stiffest, followed by the natural rubber pad and the EPDM railpad is the least stiff based on their static stiffness results. The relationships for the natural frequencies and the dynamic stiffnesses with the preload conditions are observed to increase logarithmically. However, the effect that different preloads have on the dynamic properties are different among the three rubber pads. The natural frequency and dynamic stiffness of the EPDM railpad is observed to increase steadily from 10 kN to 50 kN of preload. The natural frequency and dynamic stiffness of the natural rubber pad is observed to increase rapidly from 10 kN to 30 kN of preload and increase slowly from 30 kN to 50 kN of preload. The natural frequency and dynamic stiffness of the store bought EPDM is observed to increase slowly from 10 kN to 50 kN of preload. In terms of natural frequency and dynamic stiffness, the observations show that the EPDM railpad is affected most significantly by the different preloads, whereas the store bought EPDM has the least effect from the different preloads. The store bought EPDM achieved the highest natural

frequency and dynamic stiffness at 50 kN preload with 1425 Hz and 950.9 MN/m respectively, while the EPDM railpad achieved the lowest at 10 kN preload with 897 Hz and 376.8 MN/m respectively.

Furthermore, when comparing the results obtained from the two experiments, the dynamic stiffness of natural rubber pad at 50 kN of preload is closer to the dynamic stiffness of store bought EPDM at 50 kN of preload, which is relatively high. Whereas the static stiffness of natural rubber pad at 50 kN of compression load is closer to the static stiffness of EPDM railpad at 50 kN of preload, which is relatively low. This shows that the grooves profile of the natural rubber pad allows dissipation of stress efficiently when being compressed steadily and slowly, this is due to the grooves allowing space for the rubber to expand horizontally during compression. The natural rubber pad with grooves acts normally like other rubber pads with plane surfaces when the excitation due to instantaneous impact.

The results at preload of 20 kN make excellent comparison with the results obtained from previous studies done by other researchers. Remennikov and Kaewunruen (2005) found that at the preload of 20 kN, its new HDPE railpad with a thickness of 10 mm and plane surfaces achieved a dynamic stiffness of 628 MN/m, while Van't Zand (1994) found that at the preload of 25 kN, its new HDPE railpad with a thickness of 12 mm and plane surfaces achieved a dynamic stiffness of 375 MN/m. Note that both mentioned studies are also using instrumented hammer impact methods to analyse their railpads. Despite different materials, the EPDM railpad used in this study achieved a dynamic stiffness of 535.1 MN/m at the preload of 20 kN, which is within the range of the dynamic stiffnesses of the HDPE railpad found by previous researchers. This shows that the EPDM railpad has a dynamic stiffness that is within the operating dynamic stiffnesses of standard railpads, and it can be correctly detected by the instrumented hammer impact test rig designed for this study.

Based on the damping coefficient results, the damping coefficient of the natural rubber pad decreases steadily when the preload increases. The damping coefficient of store bought EPDM decreases rapidly from 10 kN to 20 kN of preload, increases from 20 kN to 40 kN of preload and decreases from 40

kN to 50 kN of preload. The damping coefficient of EPDM railpad increases steadily from 10 kN to 40 kN of preload, then decreases from 40 kN to 50 kN of preload. Natural rubber pad reached its highest damping coefficient at 10 kN of preload, which is 6868 Ns/m and reached its lowest damping coefficient at 50 kN of preload, which is 1719 Ns/m, the difference is equal 5149 Ns/m. Store bought EPDM reached its highest damping coefficient at 10 kN of preload, which is 4354 Ns/m and reached its lowest damping coefficient at 20 kN of preload, which is 1305 Ns/m, the difference is equal 3049 Ns/m. EPDM railpad reached its highest damping coefficient at 40 kN of preload, which is 4668 Ns/m and reached its lowest damping coefficient at 10 kN of preload, which its 2340 Ns/m, the difference is equal 2328 Ns/m. Based on these observations, the damping coefficient of natural rubber pad is affected most significantly by the different preloads, whereas the damping coefficient of EPDM railpad has the least effect from the different preloads.

CHAPTER 5

CONCLUSIONS AND RECOMMENDATIONS

5.1 Conclusions of the Study

The aim and objectives that have been proposed in this study have been achieved. A test rig that utilised the instrumented hammer impact method and based on the SDOF vibration response measurement in analysing the dynamic properties of rubber pads is developed. The test rig is found to be reliable, easy and effective in obtaining the natural frequency, dynamic stiffness and damping coefficient of rubber pads that have the size of a standard railpad. The test rig enables the application of preloads on the rubber pad during testing with a range of 10 kN to 50 kN. The effect of the different preloads on the rubber pads can be observed clearly with the help of IMC Software and ME's scope software in logging and computing the dynamic properties results. It is observed that the changing preloads has a significant effect on the dynamic properties of the rubber pads. The store bought EPDM has the highest natural frequencies and dynamic stiffnesses from 10 kN to 50 kN of preloads, it achieved the highest dynamic stiffness amongst three rubber pads at 50 kN of preload, which is 950.9 MN/m. The EPDM railpad has the lowest natural frequencies and dynamic stiffnesses from 10 kN to 50 kN of preloads, it achieved the lowest dynamic stiffness amongst three rubber pads at 10 kN of preload, which is 376.8 MN/m. The natural rubber pad achieved its highest damping coefficient at 10 kN of preload, which is 6868 Ns/m. The store bought EPDM reached its highest damping coefficient at 10 kN of preload, which is 4354 Ns/m. The EPDM railpad achieved its highest damping coefficient at 40 kN of preload, which is 4668 Ns/m. The changing preloads are observed to have the most significant effect on the damping coefficient of the natural rubber pad and have the least significant effect on the damping coefficient of the EPDM railpad.

5.2 Recommendations for Future Research

Due to the limitations faced by this study, the potential of obtaining more data to further evaluate the effect of different preloads, different material

composition and different geometry properties have on the rubber pads is greatly limited. Thus, many recommendations can be suggested to improve the quality of the results of the research topic.

First, the instrumented hammer impact experiment on the rubber pads can be repeated a few times so that the performance of the test rig in obtaining the accurate results can be evaluated. Next, the range of preloads applied on the rubber pads can be expanded to have a better observation of the effect of preloads on the dynamic properties of the rubber pads. Force sensing bolts are suggested to be used instead of normal bolts to have more accurate measurement when preloading the rubber pad. According to the study done by Kaewunruen and Remennikov (2008), the test rig developed at the University of Wollongong is capable of applying preloads up to approximately 400 kN. With the help of force sensing bolts, the dynamic properties resulting with the preload starting from the 0 kN can be obtained. This provides a better observation of the effect on the dynamic properties of the railpads at different preload conditions.

Furthermore, the HDPE railpad and the studded rubber pad used and analysed in previous studies can be acquired for this instrumented hammer impact experiment to evaluate the correlation of the results obtained with the test rig. Last but not least, the effect of the geometry properties on the dynamic properties can be investigated by conducting the instrumented hammer impact experiment on rubber pads that are made with the same material but with different surface profiles, for example, EPDM rubber pads with plane surfaces, studded surfaces and grooved surfaces.

REFERENCES

Chen, J. and Zhou, Y., 2020. Dynamic vertical displacement for ballastless track-subgrade system under high-speed train moving loads. *Soil Dynamics and Earthquake Engineering,* 129, p.105911. https://doi.org/10.1016/j.soildyn.2019.105911

Doshin Rubber Engineering, 2020. *Rail Track Isolation - DOSHIN RUBBER ENGINEERING - GO BEYOND LIMITS MAKE DREAMS REALIT.* [online] Available at: https://doshinrubber.com/rail-track-isolation/ [Accessed 23 March 2022].

Engineering ToolBox, 2018. *Bolt Torque Calculator.* [online] Available at: https://www.engineeringtoolbox.com/bolt-torque-load-calculator-d_2065.html [Accessed 11 April 2022].

He, Q., Cai, C., Zhu, S., Zhang, J. and Zhai, W., 2018. Dynamic performance of low vibration slab track on shared high-speed passenger and freight railway. *Transport,* 33(3), pp.669-678. https://doi.org/10.3846/16484142.2018.1457569

Indraratna, B., Ngo, N. and Rujikiatkamjorn, C., 2017. Improved Performance of Ballasted Rail Tracks Using Plastics and Rubber Inclusions. *Procedia Engineering,* 189, pp.207-214. https://doi.org/10.1016/j.proeng.2017.05.033

Issever, H., Aksoy, C., Sabuncu, H. and Karan, A., 2003. Vibration and its effects on the body. *Medical Principles and Practice,* 12(1), pp.34-38. https://doi.org/10.1159/000068155

kadum Abd Ali, N., Farhan, M.M. and Moosa, A.S., 2017. The Effect of Shape Factor on the Operation Periods of Anti-Vibration Rubber, *IISTE,* 17(6), pp. 437–447.

Kaewunruen, S. and Remennikov, A., 2005. Integrated field measurements and track simulations for condition assessment of railway track. *Faculty of Engineering - Papers.*

Kaewunruen, S. and Remennikov, A., 2008. An Alternative Rail Pad Tester for Measuring Dynamic Properties of Rail Pads Under Large Preloads. *Experimental Mechanics,* 48(1), pp.55-64. https://doi.org/10.1007/s11340-007-9059-3

Köse, H., 2015. *Balastsız Üstyapıda Asfalt Ve Beton Taşıyıcı Tabakaların Teknik Ve Ekonomik Yönden Karşılaştırılması* (Doctoral dissertation, Fen Bilimleri Enstitüsü).

Kumpulanjebco.com, 2010. *Kumpulan Jebco.* [online] Available at: http://www.kumpulanjebco.com/en/index.php?option=com_content&task=view&id=32&Itemid=77 [Accessed 23 March 2022].

Li, Z. et al., 2011. Simulation on performance of rubber isolator based on ANSYS, *2011 2nd International Conference on Mechanic Automation and Control Engineering, MACE 2011 - Proceedings,* (1), pp. 1608–1611. doi: 10.1109/MACE.2011.5987260. https://doi.org/10.1109/MACE.2011.5987260

Oregui, M., De Man, A., Woldekidan, M.F., Li, Z. and Dollevoet, R.P.B.J., 2016. Obtaining railpad properties via dynamic mechanical analysis. *Journal of Sound and Vibration,* 363, pp.460-472. https://doi.org/10.1016/j.jsv.2015.11.009

Ouyang, Z., Luo, Y. and Liu, Y., 2015. The Geometry Optimization of Shear-Type Track Rubber Absorber Based on Finite Element Method, *Proceedings - 2015 7th International Conference on Measuring Technology and Mechatronics Automation, ICMTMA 2015,* pp. 1216–1219. https://doi.org/10.1109/ICMTMA.2015.296

Remennikov, A. and Kaewunruen, S., 2005. Determination of dynamic properties of rail pads using an instrumented hammer impact technique.

Sainz-Aja, J., Carrascal, I., Ferreño, D., Pombo, J., Casado, J. and Diego, S., 2020. Influence of the operational conditions on static and dynamic stiffness of rail pads. *Mechanics of Materials,* 148, p.103505. https://doi.org/10.1016/j.mechmat.2020.103505

Sol-Sánchez, M., Moreno-Navarro, F. and Rubio-Gámez, M. C., 2014. The use of deconstructed tire rail pads in railroad tracks: Impact of pad thickness, *Materials and Design,* 58, pp. 198–203. https://doi.org/10.1016/j.matdes.2014.01.062

Sol-Sánchez, M., Moreno-Navarro, F. and Rubio-Gámez, M. C., 2015. The use of elastic elements in railway tracks: A state of the art review. *Construction and Building Materials,* 75, pp.293-305. https://doi.org/10.1016/j.conbuildmat.2014.11.027

Van't Zand, J., 1994. Assessment of dynamic characteristics of rail pads. *Rail Engineering International, 23*(4).

Wang, H., Rongong, J.A., Tomlinson, G.R. and Hong, J., 2010. Nonlinear static and dynamic properties of metal rubber dampers. *energy, 10*(1).

Wei, K., Liu, Z., Liang, Y. and Wang, P., 2016. An investigation into the effect of temperature-dependent stiffness of rail pads on vehicle-track coupled vibrations. *Proceedings of the Institution of Mechanical Engineers, Part F: Journal of Rail and Rapid Transit,* 231(4), pp.444-454. https://doi.org/10.1177%2F0954409716631786

Wei, K., Yang, Q., Dou, Y., Wang, F. and Wang, P., 2017. Experimental investigation into temperature- and frequency-dependent dynamic properties of high-speed rail pads. *Construction and Building Materials,* 151, pp.848-858. https://doi.org/10.1016/j.conbuildmat.2017.06.044

Wei, K., Zhang, P., Wang, P., Xiao, J. and Luo, Z., 2016. The Influence of Amplitude- and Frequency-Dependent Stiffness of Rail Pads on the Random Vibration of a Vehicle-Track Coupled System. *Shock and Vibration,* 2016, pp.1-10. https://doi.org/10.1155/2016/7674124

Xin, T., Ding, Y., Wang, P. and Gao, L., 2020. Application of rubber mats in transition zone between two different slab tracks in high-speed railway. *Construction and Building Materials,* 243, p.118219. https://doi.org/10.1016/j.conbuildmat.2020.118219

Zakeri, R. *et al.,* 2021. Influence of rubber sheet on dynamic response of machine foundations, *Construction and Building Materials*, 274, p. 121788. https://doi.org/10.1016/j.conbuildmat.2020.121788

APPENDICES

Appendix A: Diagrams

Appendix A-1:   Bottom Steel Plate in SolidWorks
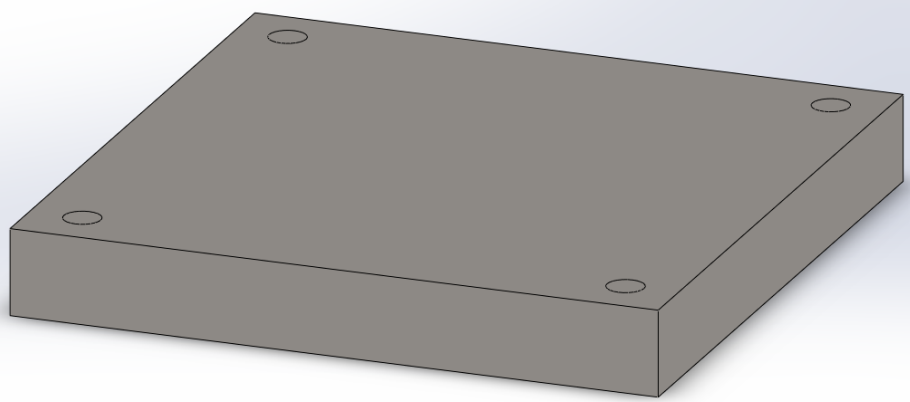
Appendix A-2:   Steel Plate (Railseat) in SolidWorks
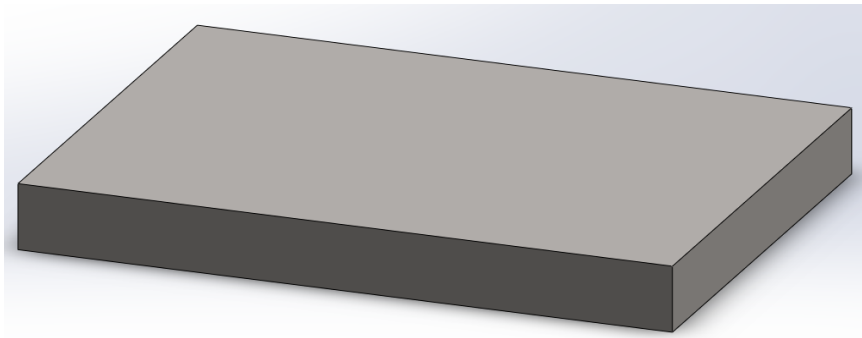
Appendix A-3:   Top Steel Plate in SolidWorks
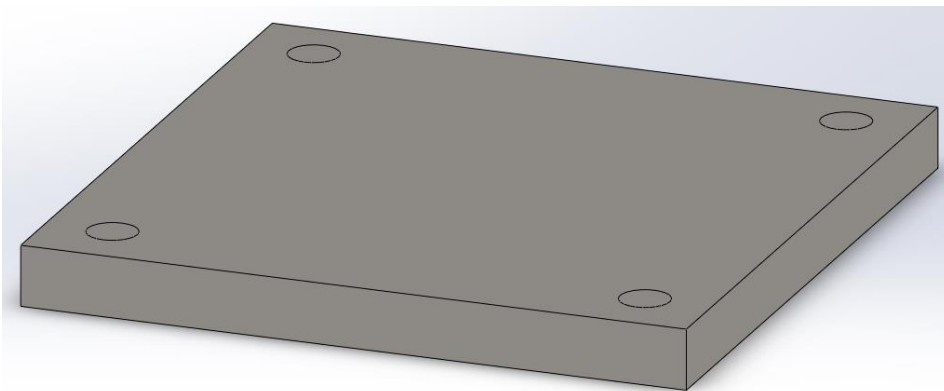
Appendix A-4:   Experiment Setup Assembled in SolidWorks
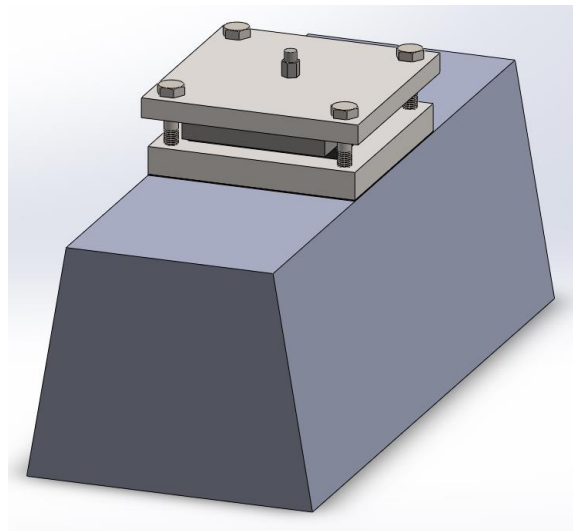
Appendix A-5:   Bottom Steel Plate

Appendix A-6:   Steel Plate (Railseat)
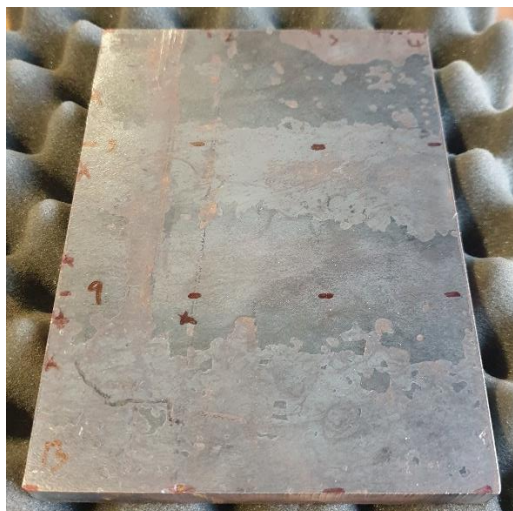
Appendix A-7:   Top Steel Plate
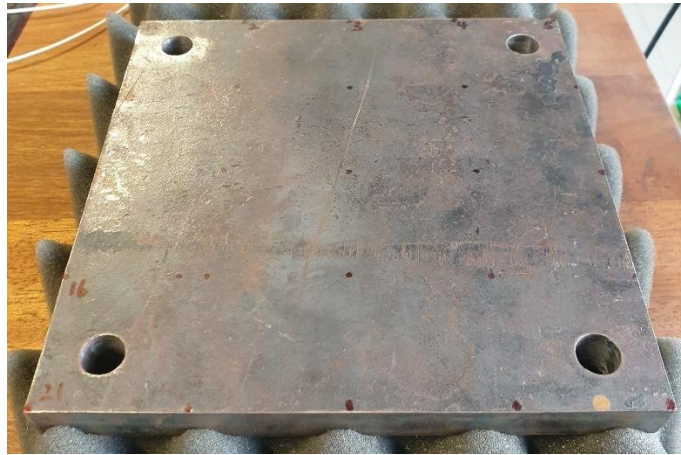
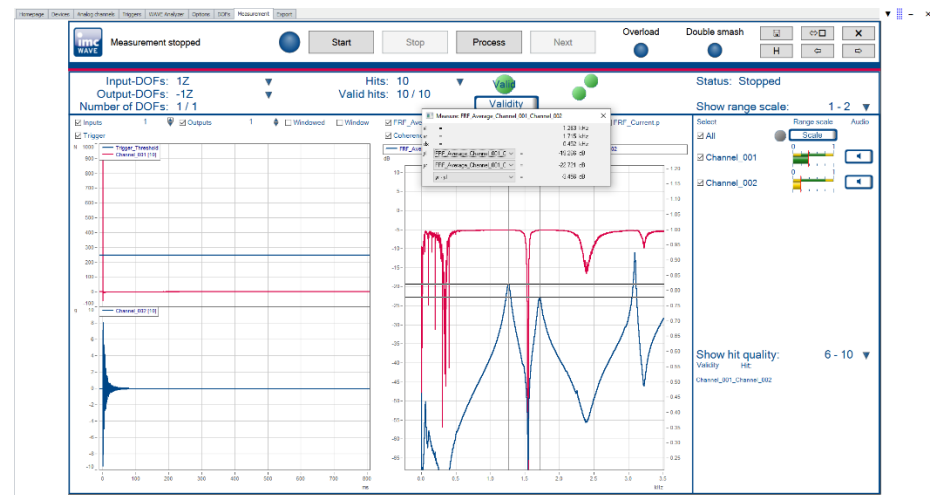Appendix A-8:   Shimadzu AGS-X 100 kN (Universal Testing Machine)
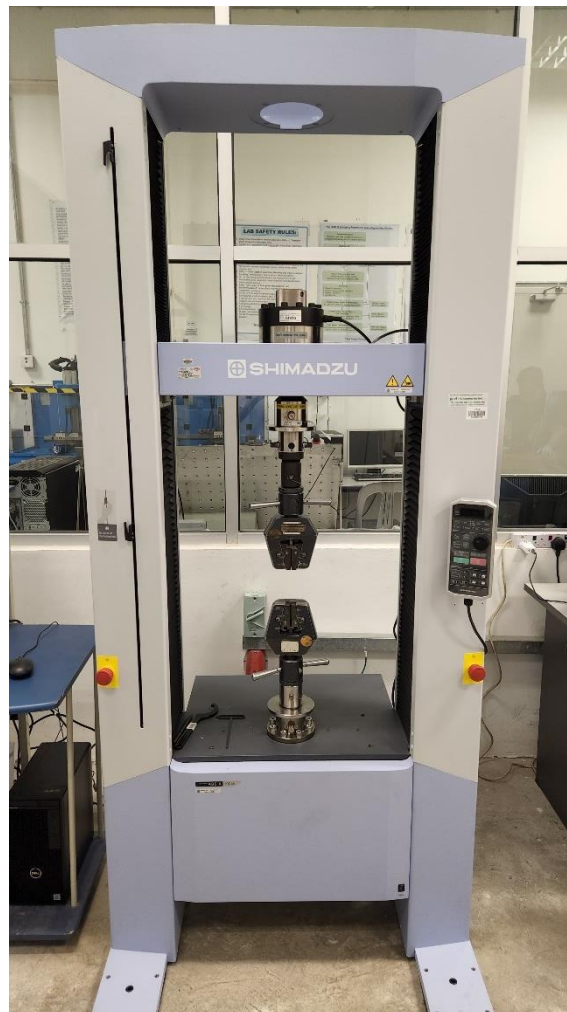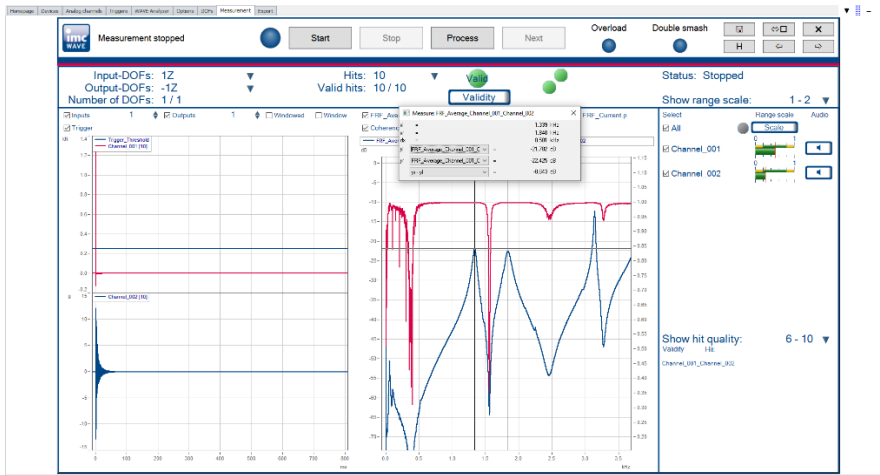
Appendix A-9:   FRF of EPDM Railpad under 20 kN Preload by IMC Software
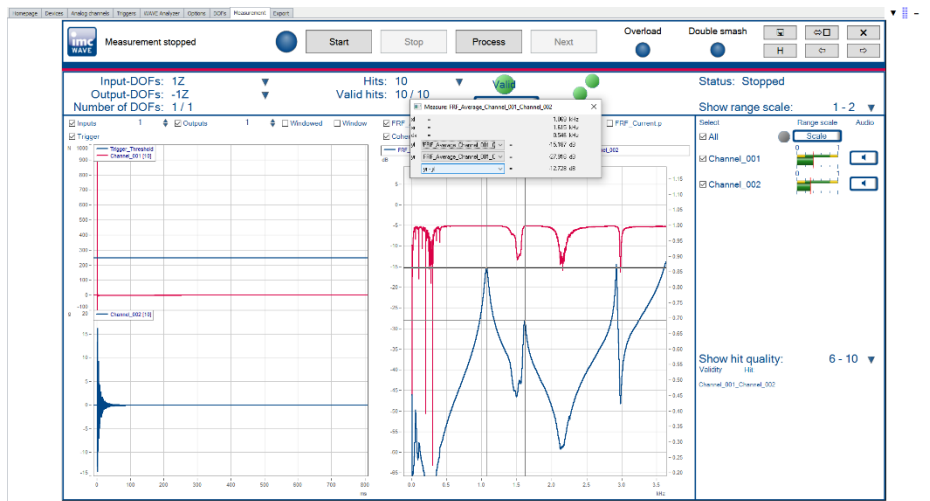
Appendix A-10:   FRF of EPDM Railpad under 30 kN Preload by IMC Software
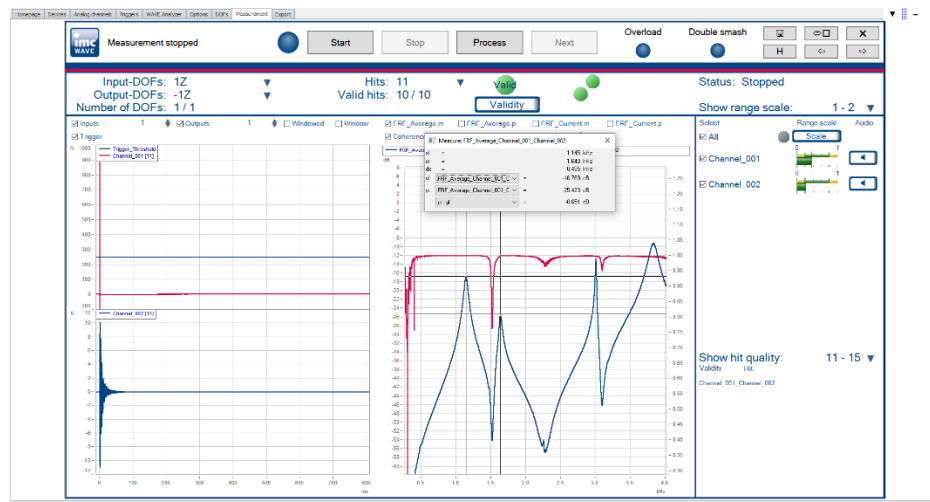
Appendix A-11:   FRF of EPDM Railpad under 40 kN Preload by IMC Software

Appendix A-12: FRF of EPDM Railpad under 50 kN Preload by IMC Software

Appendix A-13: FRF of Store Bought EPDM under 10 kN Preload by IMC Software

Appendix A-14: FRF of Store Bought EPDM under 20 kN Preload by IMC Software

Appendix A-15: FRF of Store Bought EPDM under 30 kN Preload by IMC Software
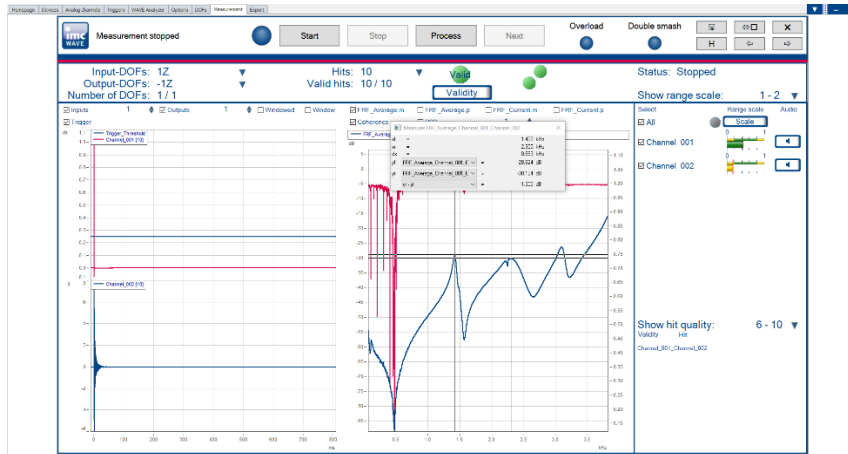
Appendix A-16: FRF of Store Bought EPDM under 40 kN Preload by IMC Software
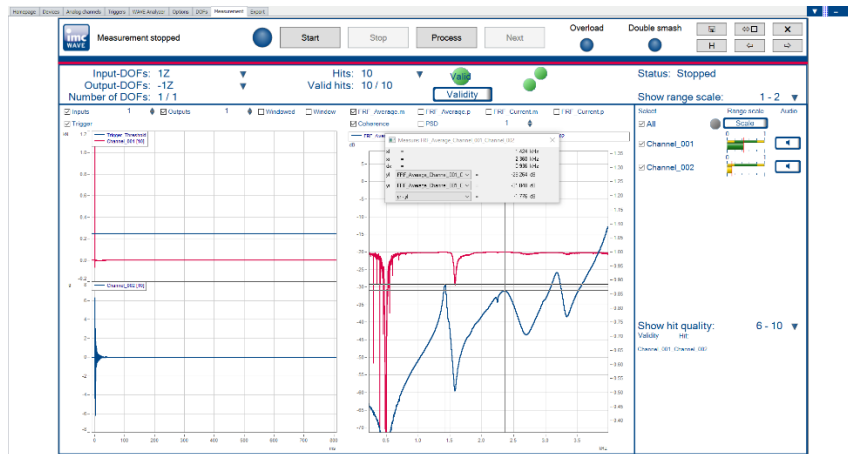
Appendix A-17: FRF of Store Bought EPDM under 50 kN Preload by IMC Software

Appendix A-18: FRF of Natural Rubber Pad under 10 kN Preload by IMC Software

Appendix A-19: FRF of Natural Rubber Pad under 20 kN Preload by IMC Software
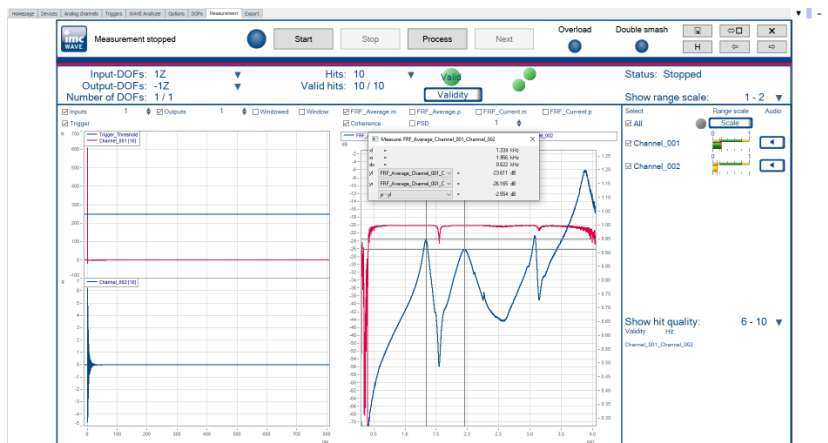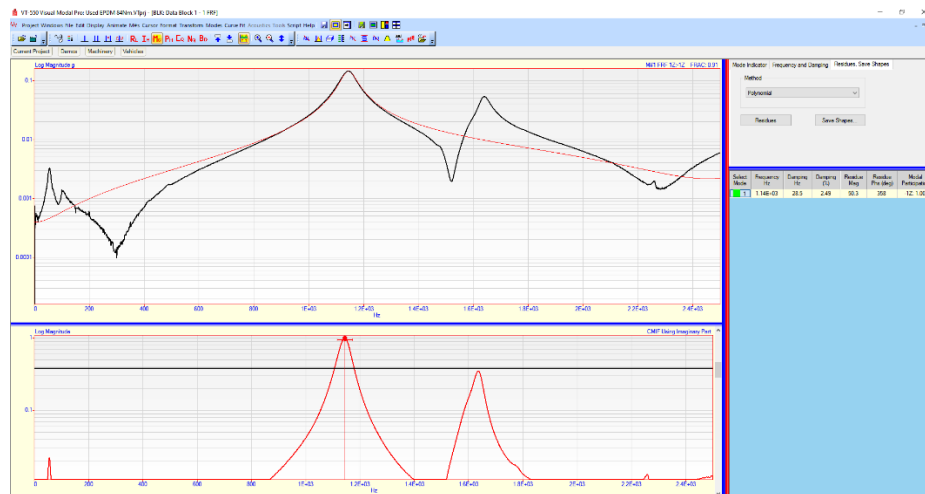

Appendix A-20: FRF of Natural Rubber Pad under 30 kN Preload by IMC Software

Appendix A-21: FRF of Natural Rubber Pad under 40 kN Preload by IMC Software
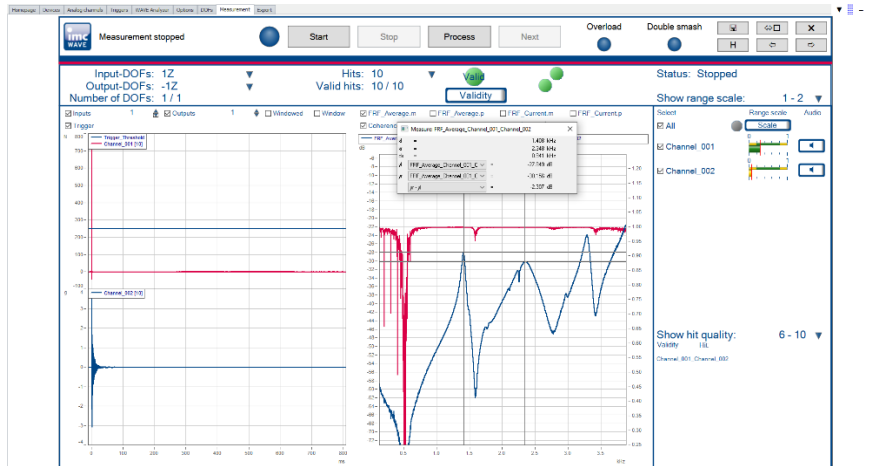
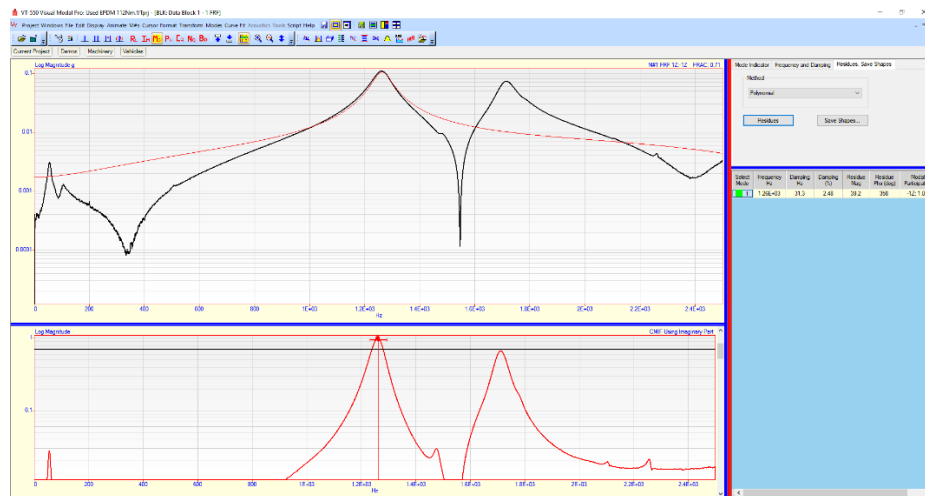Appendix A-22: FRF of Natural Rubber Pad under 50 kN Preload by IMC Software

Appendix A-23: FRF and Damping Ratio of EPDM Railpad at 20 kN Preload
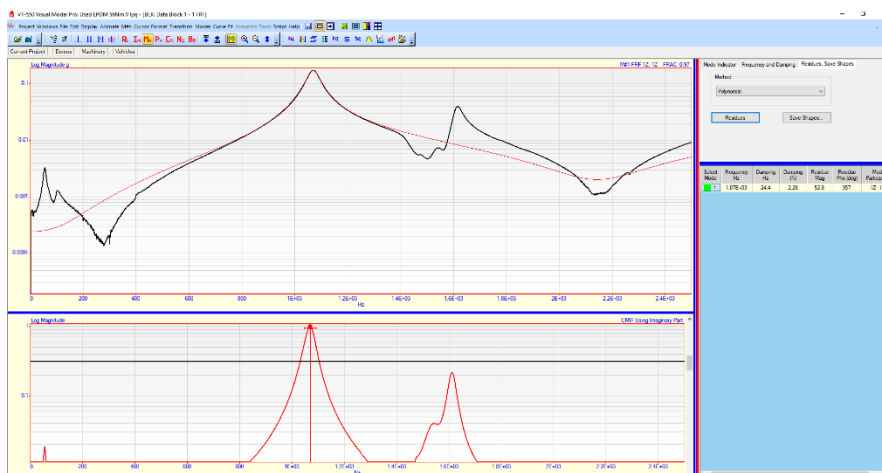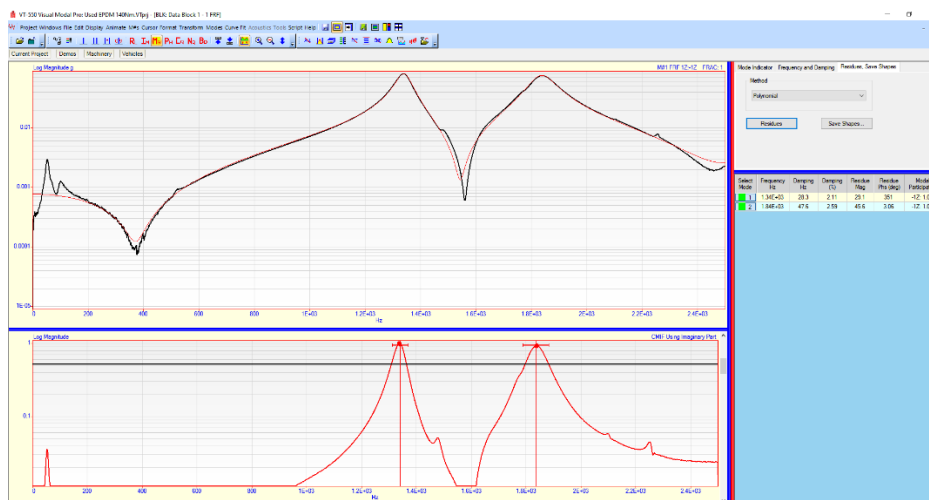
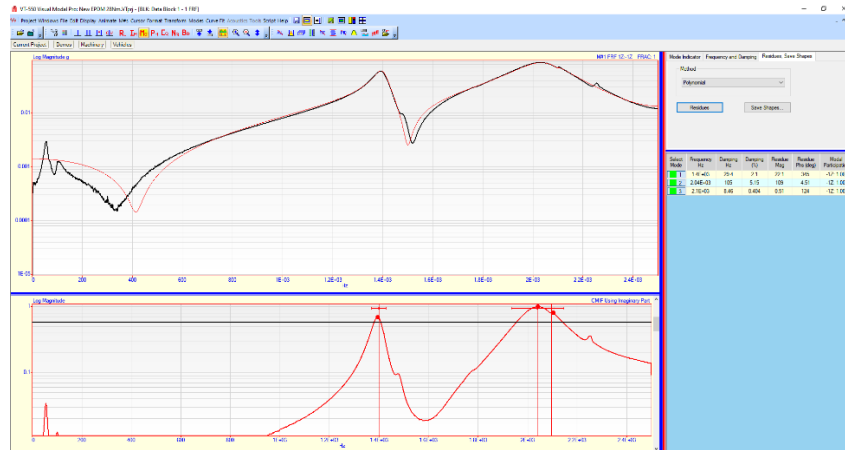Appendix A-24: FRF and Damping Ratio of EPDM Railpad at 30 kN Preload

Appendix A-25: FRF and Damping Ratio of EPDM Railpad at 40 kN Preload
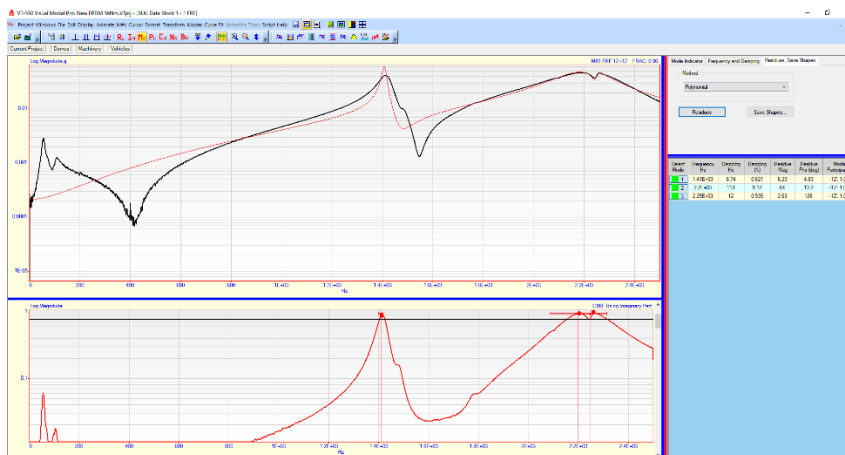

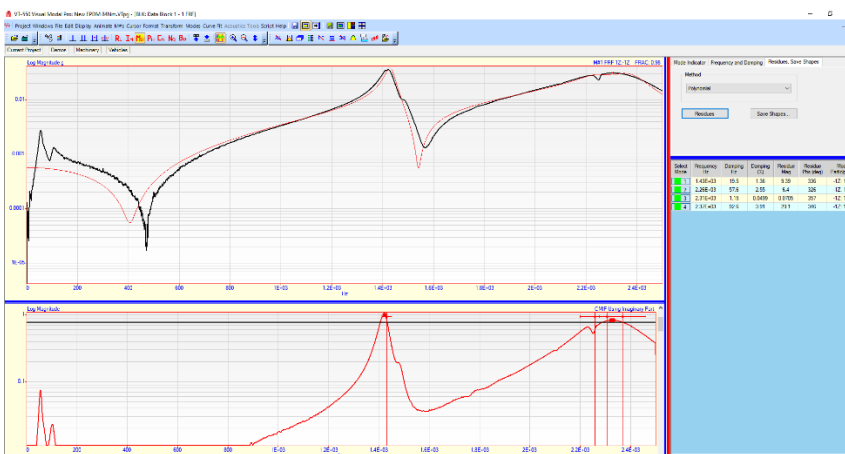Appendix A-26: FRF and Damping Ratio of EPDM Railpad at 50 kN Preload

Appendix A-27: FRF and Damping Ratio of Store Bought EPDM at 10 kN Preload
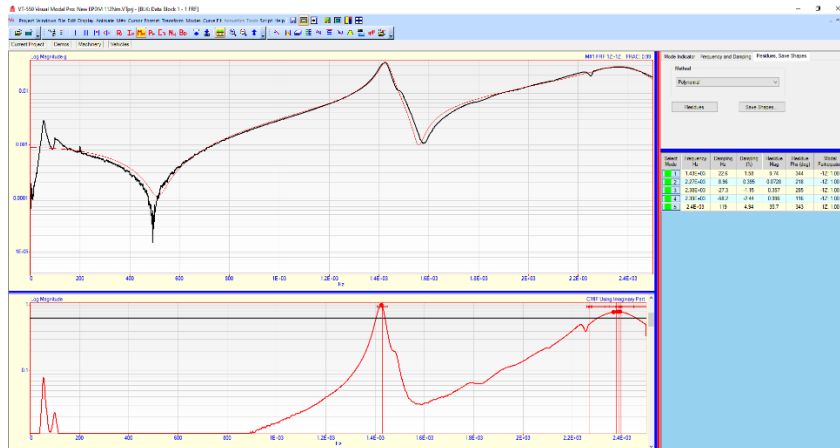

Appendix A-28: FRF and Damping Ratio of Store Bought EPDM at 20 kN Preload
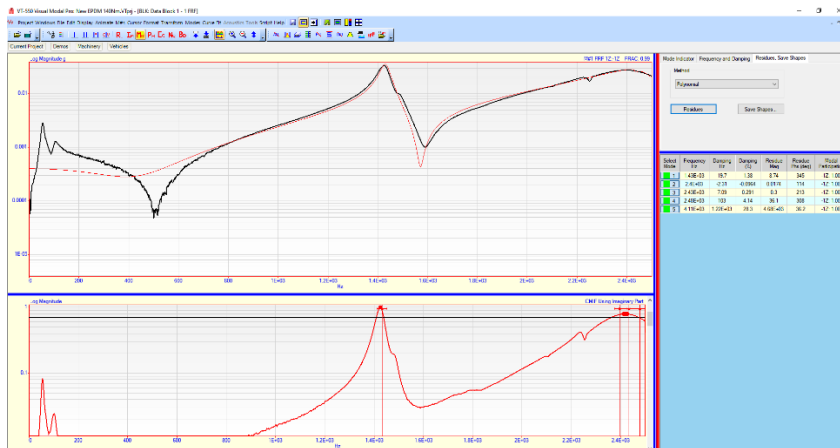

Appendix A-29: FRF and Damping Ratio of Store Bought EPDM at 30 kN Preload

Appendix A-30: FRF and Damping Ratio of Store Bought EPDM at 40 kN Preload

Appendix A-31: FRF and Damping Ratio of Store Bought EPDM at 50 kN Preload

Appendix A-32: FRF and Damping Ratio of Natural Rubber Pad at 10 kN Preload
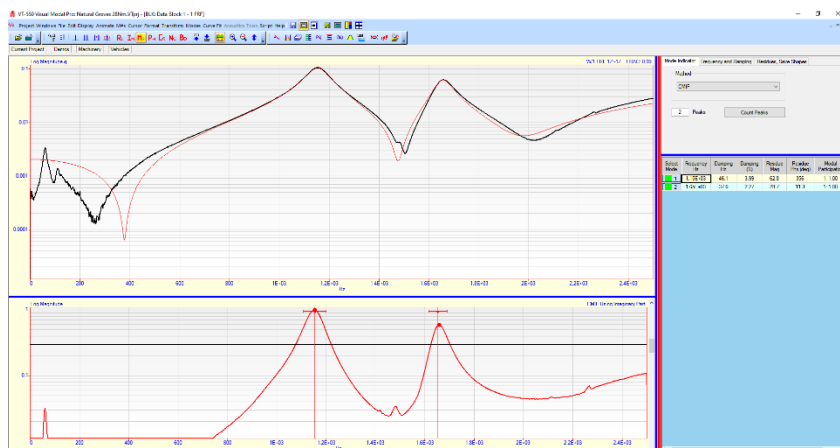
Appendix A-33: FRF and Damping Ratio of Natural Rubber Pad at 20 kN Preload

Appendix A-34: FRF and Damping Ratio of Natural Rubber Pad at 30 kN Preload
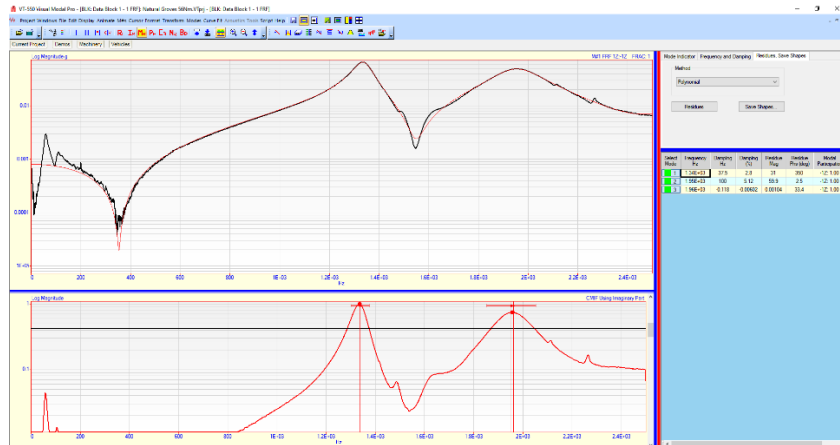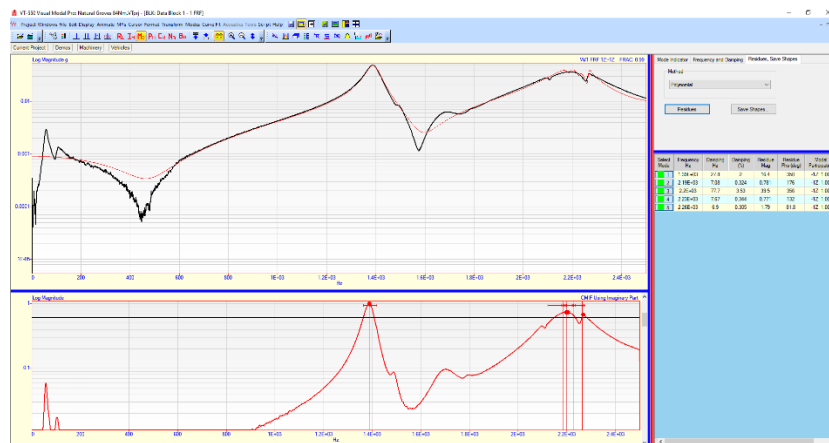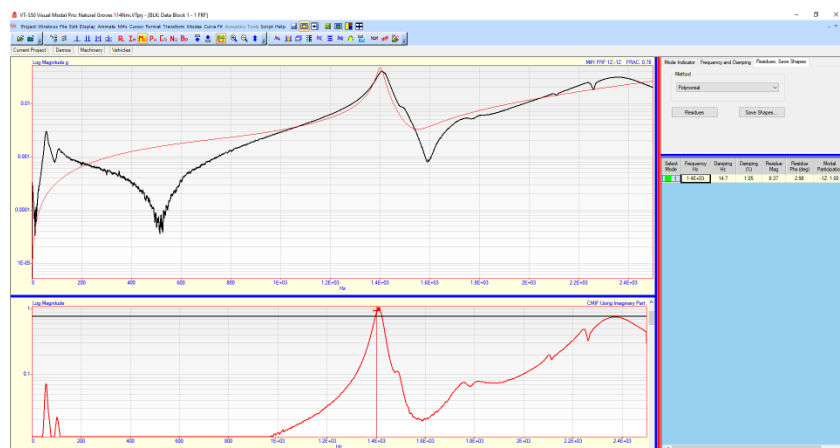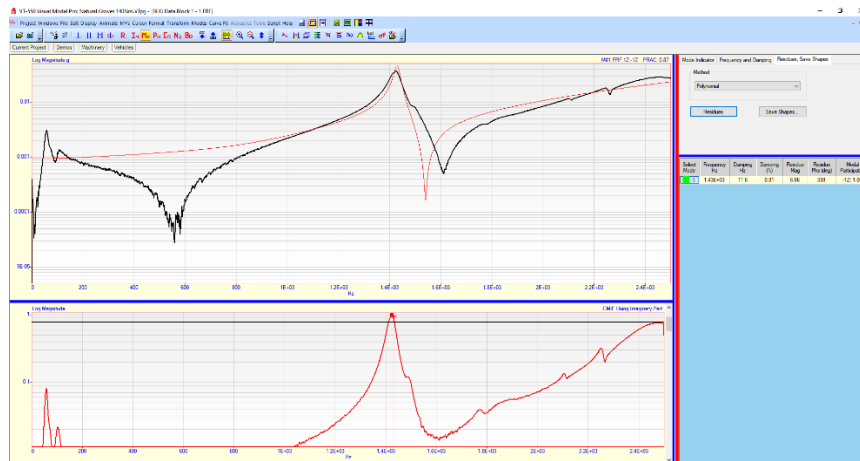

Appendix A-35: FRF and Damping Ratio of Natural Rubber Pad at 40 kN Preload

Appendix A-36: FRF and Damping Ratio of Natural Rubber Pad at 50 kN Preload

Appendix B: Tables

Appendix B-1:   Value of K with mild-steel bolts in range M8 to M24

Conditions	K value
Normal dry	0.2
Non-plated black finish	0.3
Zinc-plated	0.2
Slightly lubricated	0.18
Cadmium-plated	0.16

Appendix B-2:   Gantt Chart of the Project

Task		W1	W2	W3	W4	W5	W6	W7	W8	W9	W10	W11	W12	W13	W14
Project planning & setup design	Plan	●	●												
	Actual	●	●	●											
Materials preparation & setup assembling	Plan			●	●	●									
	Actual				●	●									
Experimentation & data collection	Plan						●	●	●						
	Actual						●	●	●						
Report writing & FYP poster design	Plan									●	●	●	●		
	Actual									●	●	●	●		
Report submission & FYP presentation	Plan													●	●
	Actual													●	●

Appendix C: Engineering Drawings

Appendix C-1:   Engineering Drawing of Bottom Steel Plate
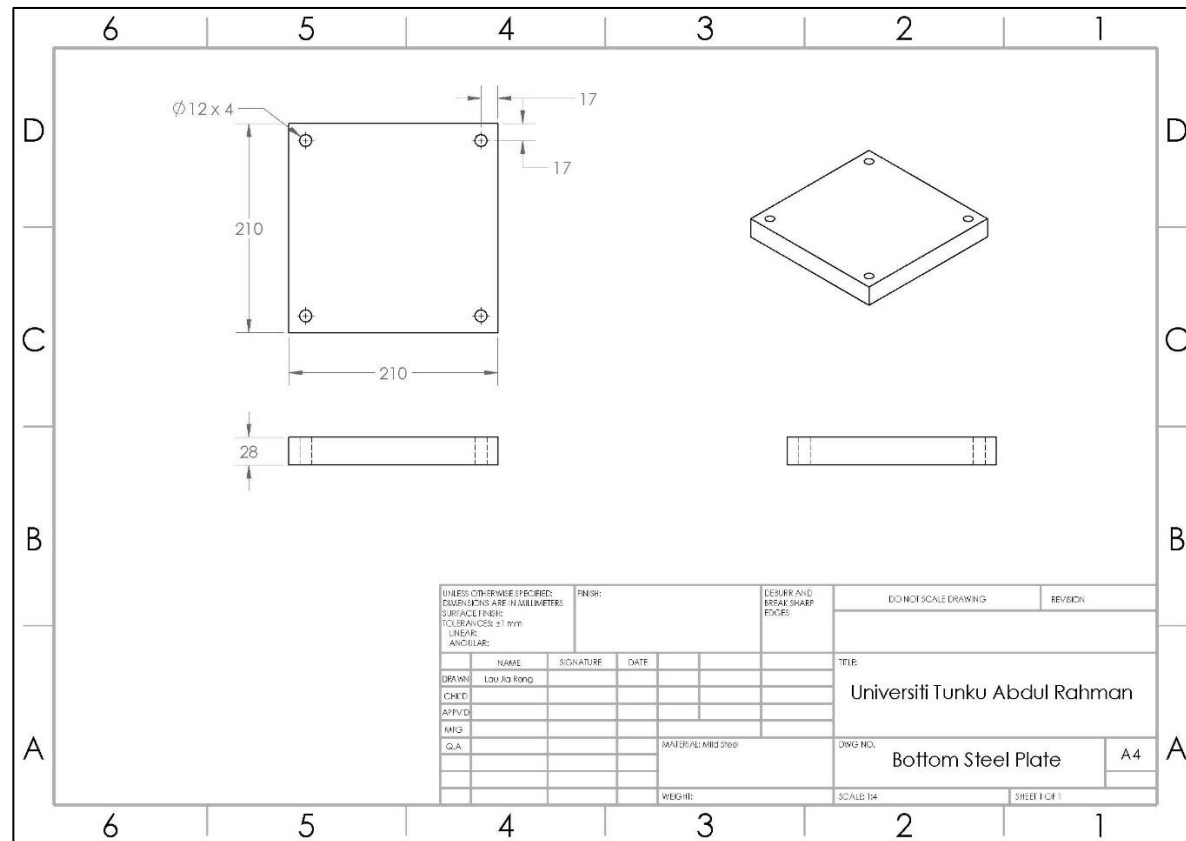
Appendix C-2:   Engineering Drawing of Steel Plate (RailSeat)

UNLESS OTHERWISE SPECIFIED: DIMENSIONS ARE IN MILLIMETERS SURFACE FINISH: TOLERANCES: ±1 mm LINEAR: ANGULAR:	FINISH:			DEBURR AND BREAK SHARP EDGES		DO NOT SCALE DRAWING	REVISION

	NAME	SIGNATURE	DATE			TITLE:	
DRAWN	Lau Jia Rong						
CHK'D						Universiti Tunku Abdul Rahman	
APPV'D							
MFG							
Q.A			MATERIAL: Mild Steel		DWG NO.	Rail Seat	A4
			WEIGHT:		SCALE:1:5		SHEET 1 OF 1
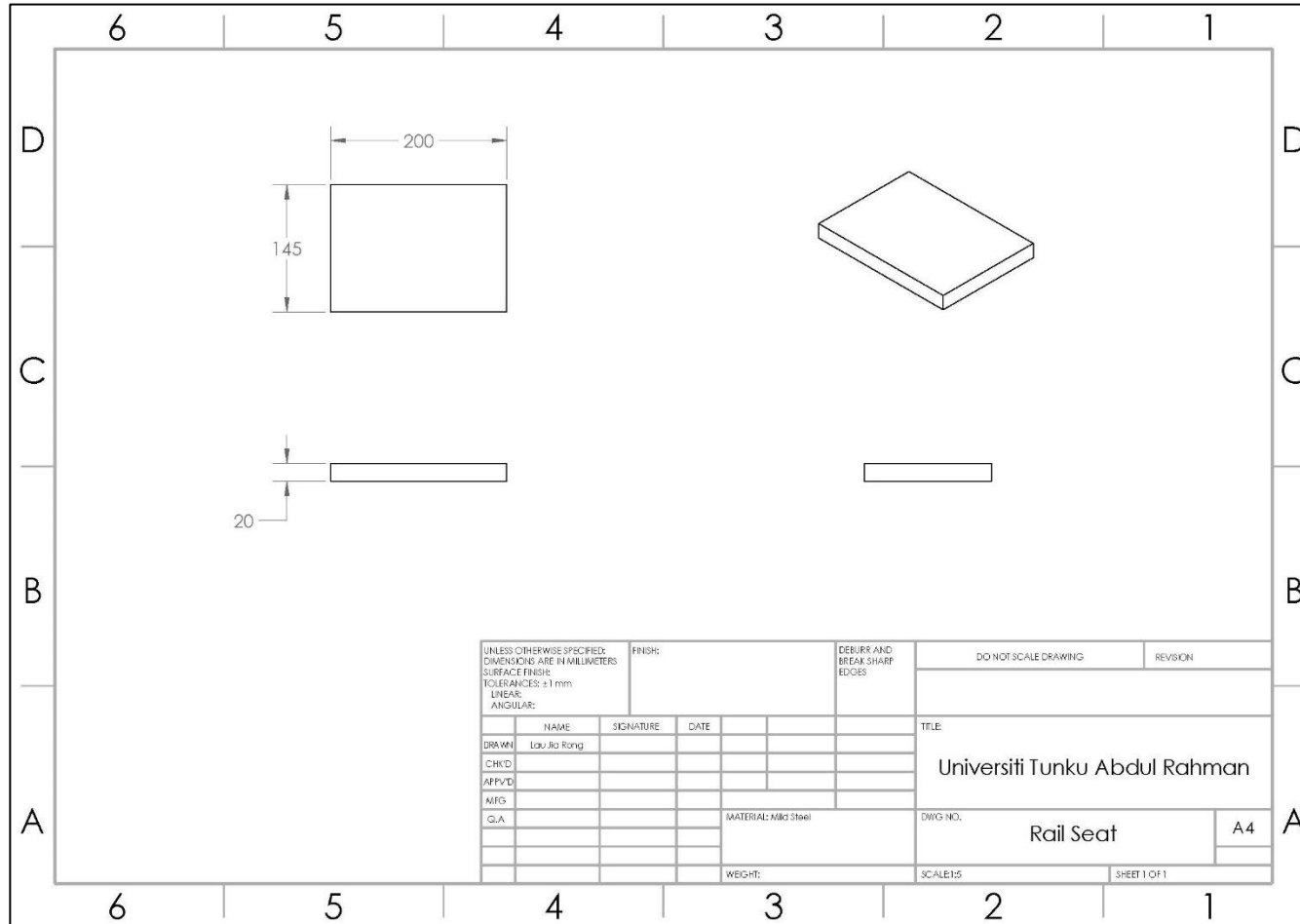
Appendix C-3:   Engineering Drawing of Top Steel Plate

| | 6 | 5 | 4 | 3 | 2 | 1 |

∅16.50 x 4

22

22

220

220

20

	NAME	SIGNATURE	DATE
DRAWN	Lau Jia Rong		
CHK'D			
APPV'D			
MFG			
Q.A			

UNLESS OTHERWISE SPECIFIED:
DIMENSIONS ARE IN MILLIMETERS
SURFACE FINISH:
TOLERANCES: ±1 mm
  LINEAR:
  ANGULAR:

FINISH:

DEBURR AND
BREAK SHARP
EDGES

DO NOT SCALE DRAWING

REVISION

TITLE:

Universiti Tunku Abdul Rahman

MATERIAL: Mild Steel

DWG NO.

Upper Plate

A4

WEIGHT:

SCALE: 1:4

SHEET 1 OF 1